Diflunisal Analogues Stabilize the Native State of Transthyretin. Potent Inhibition of Amyloidogenesis

Sara L. Adamski-Werner,[†] Satheesh K. Palaninathan,[‡] James C. Sacchettini,[‡] and Jeffery W. Kelly*[,†]

The Department of Chemistry and the Skaggs Institute of Chemical Biology, The Scripps Research Institiute, 10550 N. Torrey Pines Rd., La Jolla, California 92037, and The Department of Biochemistry and Biophysics, Texas A&M University, College Station, Texas 77843-3255

Received July 17, 2003

Analogues of diflunisal, an FDA-approved nonsteroidal antiinflammatory drug (NSAID), were synthesized and evaluated as inhibitors of transthyretin (TTR) aggregation, including amyloid fibril formation. High inhibitory activity was observed for 26 of the compounds. Of those, eight exhibited excellent binding selectivity for TTR in human plasma (binding stoichiometry >0.50, with a theoretical maximum of 2.0 inhibitors bound per TTR tetramer). Biophysical studies reveal that these eight inhibitors dramatically slow tetramer dissociation (the rate-determining step of amyloidogenesis) over a duration of 168 h. This appears to be achieved through ground-state stabilization, which raises the kinetic barrier for tetramer dissociation. Kinetic stabilization of WT TTR by these eight inhibitors is further substantiated by the decreasing rate of amyloid fibril formation as a function of increasing inhibitor concentration (pH 4.4). X-ray cocrystal structures of the TTR·**18**$_2$ and TTR·**20**$_2$ complexes reveal that **18** and **20** bind in opposite orientations in the TTR binding site. Moving the fluorines from the meta positions in **18** to the ortho positions in **20** reverses the binding orientation, allowing the hydrophilic aromatic ring of **20** to orient in the outer binding pocket where the carboxylate engages in favorable electrostatic interactions with the ϵ-ammonium groups of Lys 15 and 15′. The hydrophilic aryl ring of **18** occupies the inner binding pocket, with the carboxylate positioned to hydrogen bond to the serine 117 and 117′ residues. Diflunisal itself appears to occupy both orientations based on the electron density in the TTR·**1**$_2$ structure. Structure−activity relationships reveal that para-carboxylate substitution on the hydrophilic ring and dihalogen substitution on the hydrophobic ring afford the most active TTR amyloid inhibitors.

Introduction

Amyloid diseases appear to be caused by the deposition of any one of more than 20 nonhomologous human proteins or protein fragments, ultimately affording a fibrillar cross-β-sheet quaternary structure. Formation of amyloid fibrils from a normally folded protein like transthyretin requires protein misfolding to produce an assembly competent intermediate.[1−3] The process of transthyretin (TTR) amyloidogenesis appears to cause three different amyloid diseases: senile systemic amyloidosis (SSA), familial amyloid polyneuropathy (FAP), and familial amyloid cardiomyopathy (FAC).[4−6] SSA is associated with the deposition of wild-type TTR, while FAP and FAC are caused by the amyoidogenesis of one of over 80 TTR variants.[7,8]

TTR is a 55 kDa homotetramer characterized by 2,2,2 symmetry, having two identical funnel-shaped binding sites at the dimer−dimer interface, where thyroid hormone (T4) can bind in blood plasma and CSF (Figure 1).[9,10] In addition, transthyretin is typically bound to less than 1 equiv of holo retinol binding protein.[11] TTR misfolding including tetramer dissociation into monomers followed by tertiary structural changes within the monomer render the protein capable of misassembly, ultimately affording amyloid.[2,12] The only treatment currently available for FAP employs gene therapy mediated by liver transplantation to replace variant TTR in the blood with the WT protein.[13−16] This approach will likely not be effective for FAC due to the continued deposition of WT TTR,[15−17] nor would it be useful for the treatment of SSA, where the process of WT TTR deposition appears to be causative.[4] Liver transplantation therapy would also fail for approximately 10 of the TTR variants that deposit amyloid fibrils in the leptomeninges leading to CNS disease, as this TTR is synthesized by the choroid plexus. Hence, it is desirable to develop a general noninvasive small molecule-based therapeutic strategy.

Previous studies demonstrate that TTR misfolding leading to amyloid fibril formation can be prevented by T4-mediated stabilization of the tetramer.[18] Recently we discovered several structurally diverse families of small molecule tetramer stabilizers that bind to one or both T4 sites within TTR and prevent amyloidosis without the likely side effects of the hormone T4.[19−22] These compounds include several nonsteroidal antiinflammatory drugs (NSAIDS) such as flufenamic acid,[22] diclofenac,[24] flurbiprofen,[19] and diflunisal (**1**),[19] that appear to function by increasing the kinetic barrier associated with tetramer dissociation through ground-state binding and stabilization.[25] Because TTR is the secondary carrier of T4 in blood plasma, greater than 95% of TTR's T4 binding capacity remains un-

* To whom correspondence should be addressed. Phone: (858) 784-9601. Fax: (858) 784-9610. E-mail: jkelly@scripps.edu.
[†] The Scripps Research Institiute.
[‡] Texas A&M University.

10.1021/jm030347n CCC: $27.50
Published on Web 12/11/2003

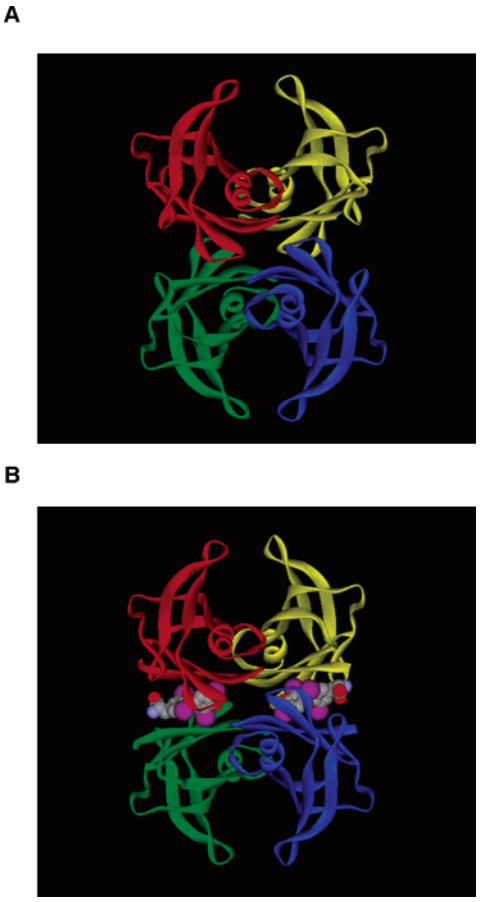

Figure 1. The X-ray crystal structure of TTR with each 127 amino acid-containing monomer shown in a different color (A), and the X-ray cocrystal structure of TTR with thyroxine (T4) occupying the two hormone binding sites (B).[10] PDB accession code: 2ROX.

utilized,[26,27] allowing for administration of tetramer stabilizers that target these sites. Diflunisal (**1**) is an FDA-approved cyclooxygenase inhibitor; hence, long-term administration could lead to gastrointestinal side effects.[28] Therefore, the ultimate goal of this work is to provide analogues of diflunisal that lack NSAID activity, but possess a high affinity for TTR in blood plasma. The first step toward this goal is the design and synthesis of diflunisal analogues as inhibitors of TTR amyloid fibril formation.

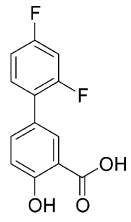

Diflunisal (1)

Binding of Small Molecules to TTR. The subunits of the TTR tetramer are interchanged by three perpendicular C_2-axes, Figure 2. The two equivalent T4 binding sites created by the quaternary structural interface are also interchanged by the two C_2 axes that are perpendicular to the crystallographic C_2 axis of symmetry. Each T4 binding site can be divided into an inner and outer binding cavity.[24,29] The inner binding cavity

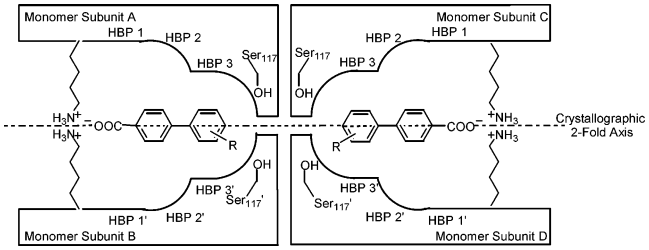

Figure 2. Schematic representation of the TTR·small molecule binding sites, demonstrating the forward binding mode where the inhibitor carboxylate participates in electrostatic interactions with the ϵ-ammonium of Lys 15 and 15′. The TTR monomer subunits are interchanged by three perpendicular C_2 axes, and two equivalent binding sites are created by the quaternary structural interface and interchanged by two C_2 axes perpendicular to the C_2 crystallographic axis of symmetry. The inner binding cavity is comprised of a pair of halogen binding pockets (HBPs 3 and 3′), and the Ser 117 and 117′ residues. The outer binding cavity consists of HBPs 1 and 1′, with HBPs 2 and 2′ at the interface of the inner and outer cavities. Lys 15 and 15′ residues define the outermost region of the outer binding cavity.

comprises a pair of halogen binding pockets (HBP), designated HBP 3 and 3′, made up by the side chains of Leu 17, Ala 108, Val 121, and Thr 119. The convergence of four Ser 117 side chains from each subunit defines the innermost region and interface between the two identical binding sites. The serine 117 hydroxyl groups can serve as hydrogen bond donors or acceptors to complimentary functionality on the small molecule or mediate electrostatic interactions with the small molecule through water molecules. The outer binding site is composed of HBP 1 and 1′, while HBP 2 and 2′ are positioned at the interface of the inner and outer binding cavities. The Lys 15 and 15′ ϵ-ammonium groups define the very outer reaches of the outer binding cavity, allowing for electrostatic interactions with small molecule anionic substituents.[19] Many of the TTR tetramer-stabilizing compounds bind in what is referred to as the forward binding mode, where an anionic substituent on the hydrophilic phenyl ring positioned in the outer binding pocket engages in an electrostatic interaction with the Lys 15 ϵ-ammonium groups. In this binding mode, the hydrophobic phenyl ring (often substituted with halogens) prefers the inner binding pocket.[19,24] However, examples of binding in the opposite orientation, the reverse binding mode, have been observed, where the hydrophilic aromatic ring is positioned in the inner cavity, allowing the carboxylate to hydrogen bond with Ser 117 and Ser 117′. In the reverse binding mode the halogen-substituted hydrophobic ring is positioned in the outer cavity.[24]

TTR (3.6 μM) amyloid fibril inhibition by diflunisal (3.6 μM) reduces acid-mediated amyloidogenesis (pH 4.4, 72 h, 37 °C) by 63%. Doubling the diflunisal concentration (7.2 μM) reduces amyloidogenesis by 97%. Diflunisal is one of the better amyloid fibril inhibitors reported to date, hence analogues of diflunisal were prepared to improve on, and understand, the facets of diflunisal's structure that make it a good inhibitor. Furthermore, orally administered diflunisal is highly bioavailable affording a sustained plasma concentration exceeding 100 μM at a dose of 250 mg twice daily.[28,30,31]

Results

Design of Diflunisal Analogues. Analogues of diflunisal characterized by subtle structural changes were prepared to evaluate structure−activity relationships as they pertain to TTR amyloid inhibition. The substitution patterns and the number of substituents including halogens, carboxylates, and hydroxyls were varied. Structure−activity data from other compound classes reveal that a carboxylate substituent or analogous anionic or H-bonding group appears to be important, possibly participating in electrostatic interactions with the ϵ-ammonium groups of Lys 15 and 15′ or hydrogen bonding interactions with Ser 117 and 117′, while the halogen-substituted hydrophobic ring compliments TTR's halogen binding pockets.[19] Both fluorine- and chlorine-substituted aryls were evaluated, including 2-fluoro, 4-fluoro, 3,5-difluoro, 2,4-difluoro, and 2,6-difluoro. Iodine-containing rings were not pursued due to their lability and potential for being thyroxine agonists. The carboxylate (anionic) substituent was removed completely in some analogues to evaluate its influence on fibril inhibition and plasma binding selectivity. Substrates containing an aldehyde or alcohol functionality were synthesized to evaluate the influence of a noncharged hydrogen bond acceptor or donor on binding selectivity and amyloid fibril inhibition, Table 1. The gem diol form of the aldehyde may be the principle binding species, although this has not been confirmed experimentally.

Synthesis of Diflunisal Analogues. The biphenyl-based diflunisal analogues were assembled using a Pd-mediated Suzuki coupling between an aryl halide and an aryl boronic acid.[32] The synthesis of analogues **2**−**10** was achieved by acetylation of either 3- or 4-iodophenol with acetic anhydride and pyridine, followed by Suzuki coupling with the appropriate fluorophenyl or phenyl boronic acid under the standard Suzuki coupling reaction conditions, Scheme 1.[32−34] Removal of the ester with Na^0 and MeOH (Zemplén conditions) provided phenols **2**−**10**.[35]

Diflunisal analogue **11** was synthesized using solid-phase methods, Scheme 2. 3-Iodobenzoic acid was coupled to Wang resin via an ester linkage, affording the resin-bound phenyl iodide, which was then coupled to 2,4-difluorophenyl boronic acid and cleaved from the resin with a 1:1 mixture of TFA:CH_2Cl_2.[36]

Carboxylate-containing substrates **12**−**22** were assembled by coupling of either methyl 3-bromobenzoate or methyl 4-bromobenzoate (both commercially available) with the appropriate fluorophenyl boronic acid utilizing standard Suzuki coupling conditions (vide supra), Scheme 3.[32−34] The ester was then saponified with LiOH·H_2O to provide the corresponding carboxylate.

5-Iodosalicylic acid was esterified using TMS−CH_2N_2, and the phenol was converted into a methyl ether employing MeI.[37] The protected salicylic acid was coupled with the various fluorophenyl boronic acids and subsequently deprotected by LiOH·H_2O saponification and BBr_3 demethylation to provide salicylic acid derivatives **23**−**27**, Scheme 4.[38]

3′,5′-Dihalo-4′-hydroxyl-containing analogues **28**−**31** were synthesized by first protecting the commercially available bromophenol as the methyl ether (MeI and K_2CO_3).[37] Suzuki coupling with a methoxycarbonylphenyl boronic acid resulted in the formation of the fully protected biphenyl substrates.[32−34] BBr_3-mediated methyl ether cleavage and saponification with LiOH·H_2O provided the fully functionalized diflunisal analogues **28**−**31**, Scheme 5.[38]

Methyl ether and methyl ester analogues of diflunisal were synthesized by either etherification with MeI and K_2CO_3 (**32**)[37] or esterification of the carboxylic acid with TMS-diazomethane to provide **33**, Scheme 6.

A series of halogenated biphenyls **34**−**38** were assembled by Suzuki coupling of iodobenzene with a series of halogen-containing boronic acids, Scheme 7.[32−34]

Table 1. TTR Amyloidogenesis Inhibition Activity of Compounds **1**−**55**, Employing an Acid-Mediated (pH 4.4) WT TTR Amyloid Fibril Formation Assay Where % Fibril Formation Is Assessed by Turbidity[a]

compound no.	% fibril formation (3.6 μM inhibitor)	% fibril formation (7.2 μM inhibitor)	plasma selectivity (equiv bound)
diflunisal (**1**)	37.0	3.4	0.13 ± 0.02
2		31.5	
3		32.4	
4[63]		46.3	
5[63]		53.1	
6[64]		19.5	
7[64]		19.6	
8	40.9	10.2	0.18 ± 0.05
9		16.4	
10		61.2	
11	39.4	9.1	none observed
12	32.6	2.6	0.20 ± 0.05
13[65]		15.7	
14[66−68]		13.3	
15	39.4	9.8	none observed
16	32.4	4.8	0.08 ± 0.00
17	35.7	5.6	0.23 ± 0.00
18	35.7	3.7	1.27 ± 0.12
19	35.1	6.7	0.29 ± 0.12
20	28.5	4.5	0.50 ± 0.05
21		30.8	
22	51.5	14.3	0.08 ± 0.01
23	38.7	2.6	0.09 ± 0.00
24	38.7	2.5	0.07 ± 0.02
25	35.5	1.0	none observed
26	29.9	3.6	0.27 ± 0.02
27	47.4	15.4	none observed
28	38.5	3.5	none observed
29	31.7	3.4	0.07 ± 0.02
30	25.5	4.4	0.12 ± 0.02
31	25.8	3.8	0.26 ± 0.04
32		69.9	
33		38.5	
34[69,70]		100.0	
35		100.0	
36		99.4	
37[71]		100.0	
38[72,73]		52.2	
39	30.6	4.4	1.30 ± 0.15
40		25.4	
41	34.5	7.1	1.96 ± 0.11
42[74,75]		35.4	
43		93.5	
44[76]		72.5	
45	32.7	3.0	0.80 ± 0.08
46	41.2	4.9	1.56 ± 0.01
47		45.4	
48	30.0	3.3	0.89 ± 0.09
49	38.9	5.9	0.54 ± 0.10
50	33.6	7.7	none observed
51[77,78]		85.5	
52[79,80]		100.0	
53[81]		81.0	
54		64.3	
55		69.6	

[a] WT TTR amyloidogenesis after 72 h incubation is defined as 100%. The error in the fibril formation assays is ±5%.

Scheme 1. Synthesis of Hydroxylated Biphenyl Inhibitors Utilizing a Pd-Mediated Suzuki Coupling

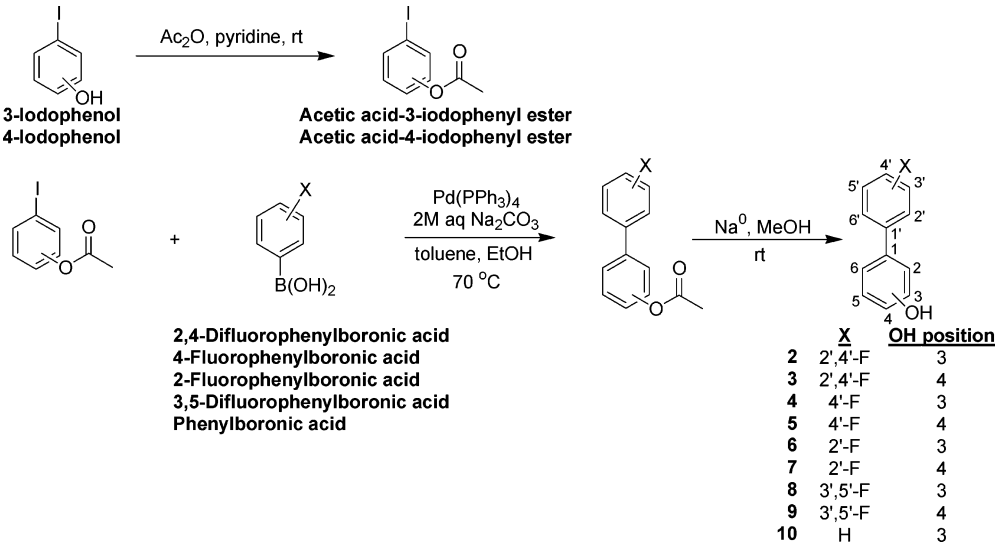

	X	OH position
2	2',4'-F	3
3	2',4'-F	4
4	4'-F	3
5	4'-F	4
6	2'-F	3
7	2'-F	4
8	3',5'-F	3
9	3',5'-F	4
10	H	3

Scheme 2. Solid-Phase Synthesis of a Diflunisal Analogue

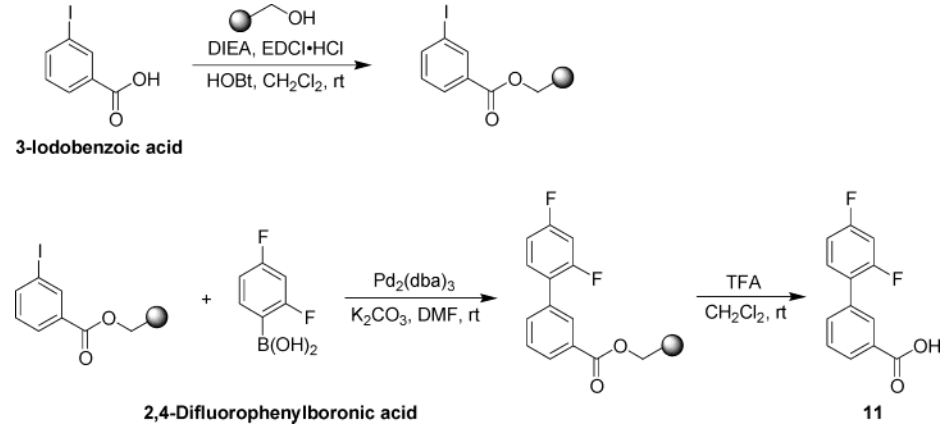

Chlorinated biaryl aldehydes **39**−**41** were assembled using 3,5-dichloroiodobenzene and either 2-, 3-, or 4-formylphenyl boronic acid, Scheme 8.[32−34] Aldehydes **42**−**44**, lacking the halogen substitution, were prepared analogously. Aldehydes **39**−**41** were either oxidized with $KMnO_4$ in acetone/water to provide the corresponding carboxylic acids **45**−**47**[39] or reduced with $NaBH_4$ in MeOH to provide the corresponding benzyl alcohols **48**−**50**, Scheme 8.[40] Reduction of the non-chlorinated aldehydes **42**−**44** with $NaBH_4$ and MeOH produced the biphenyl benzylic alcohols **51**−**53**.

3′,5′-Difluoroformyl-functionalized biphenyls **54** and **55** were synthesized via Suzuki coupling of 3,5-difluorophenyl boronic acid with either 2- or 3-iodobenzaldehyde, Scheme 9.[32−34] All other inhibitors were synthesized by similar methods and reported previously. Compounds **10**, **21**, **35**, **36**, and **43** are commercially available.

Amyloid Inhibitory Activities of the Diflunisal Analogues. The compounds described were evaluated as TTR amyloid fibril inhibitors using a previously reported turbidity assay.[24] WT TTR amyloidosis was initiated by acidification of TTR preincubated with small molecule inhibitor (25 °C, 30 min), employing buffer addition to jump the pH to a final value of 4.4. After incubation of each mixture for 72 h (37 °C), the turbidity was measured at 350 and 400 nm using a UV−vis spectrometer. All amyloid fibril formation data was normalized to WT TTR amyloidogenesis in the absence of inhibitor, assigned to be 100% fibril formation. Therefore, 5% fibril formation corresponds to a compound inhibiting 95% of WT TTR fibril formation after 72 h. Each potential inhibitor was first evaluated at a concentration of 7.2 μM relative to a TTR tetramer concentration of 3.6 μM. Compounds allowing less than 15% fibril formation were reevaluated at a concentration equal to the TTR concentration (3.6 μM) to select for the inhibitors with the highest efficacy. Fibril formation of less than 40% under these conditions is characteristic of a very good inhibitor, whereas 40−70% inhibition is indicative of a modest compound. Fibril formation data is presented in Table 1.

Plasma Selectivity of the Diflunisal Analogues. Inhibitors that keep TTR fibril formation below 50% at a concentration equal to that of TTR (3.6 μM) were further evaluated for their ability to bind TTR selectively over all other proteins in blood plasma.[41] The diflunisal concentration in blood can exceed 30 μM 20 h after a single 500 mg dose, or 300 μM 4 h after the same dose.[31,42] While this high sustained plasma concentration suggests excellent bioavailability, more selective inhibitors will allow for lower dosing and potentially fewer side-effects; therefore, human plasma was incubated with this subset of inhibitors at a final concentra-

Scheme 3. Synthesis of Carboxylate-Containing Diflunisal Analogues Utilizing a Suzuki Coupling

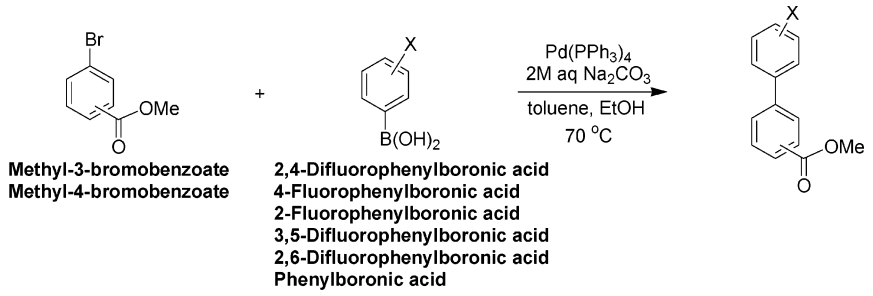

Methyl-3-bromobenzoate
Methyl-4-bromobenzoate

2,4-Difluorophenylboronic acid
4-Fluorophenylboronic acid
2-Fluorophenylboronic acid
3,5-Difluorophenylboronic acid
2,6-Difluorophenylboronic acid
Phenylboronic acid

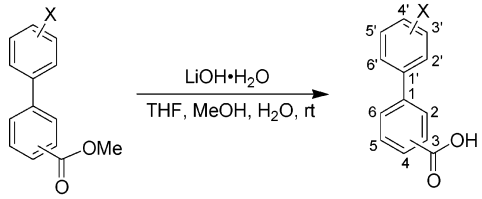

	X	CO_2H position
12	2',4'-F	4
13	4'-F	3
14	4'-F	4
15	2'-F	3
16	2'-F	4
17	3',5'-F	3
18	3',5'-F	4
19	2',6'-F	3
20	2',6'-F	4
21	H	3
22	H	4

Scheme 4. Synthesis of Salicylate-Containing Biphenyls

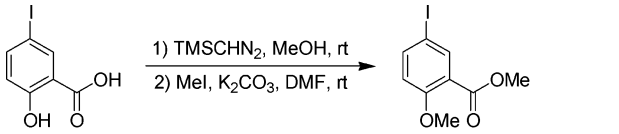

Methyl-5-iodo-2-methoxybenzoate

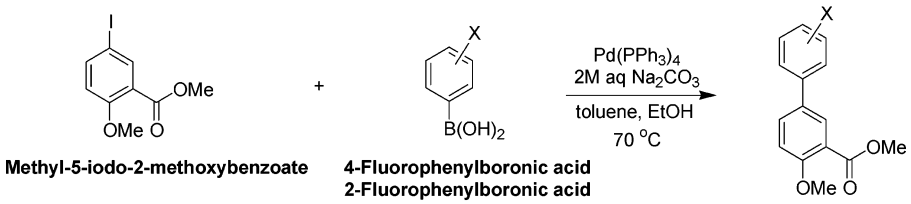

Methyl-5-iodo-2-methoxybenzoate

4-Fluorophenylboronic acid
2-Fluorophenylboronic acid
3,5-Difluorophenylboronic acid
2,4-Dichlorophenylboronic acid
Phenylboronic acid

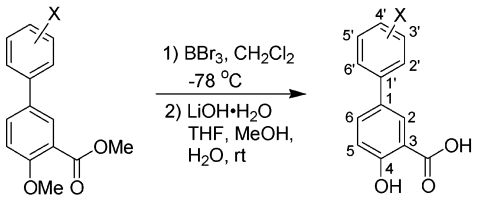

	X
23	4'-F
24	2'-F
25	3',5'-F
26	2',4'-Cl
27	H

tion of 10.8 μM (average TTR concentration in human plasma is approximately 5 μM).[31] TTR was then captured using a resin-bound antibody, and the immobilized TTR was washed three times with a solution of TSA (Tris saline)/0.05% saponin, followed by two washes with TSA.[41] The TTR−small molecule complex was

Scheme 5. Synthesis of 3′,5′-Dihalo-4′-hydroxyl Biphenyl-Containing Inhibitors

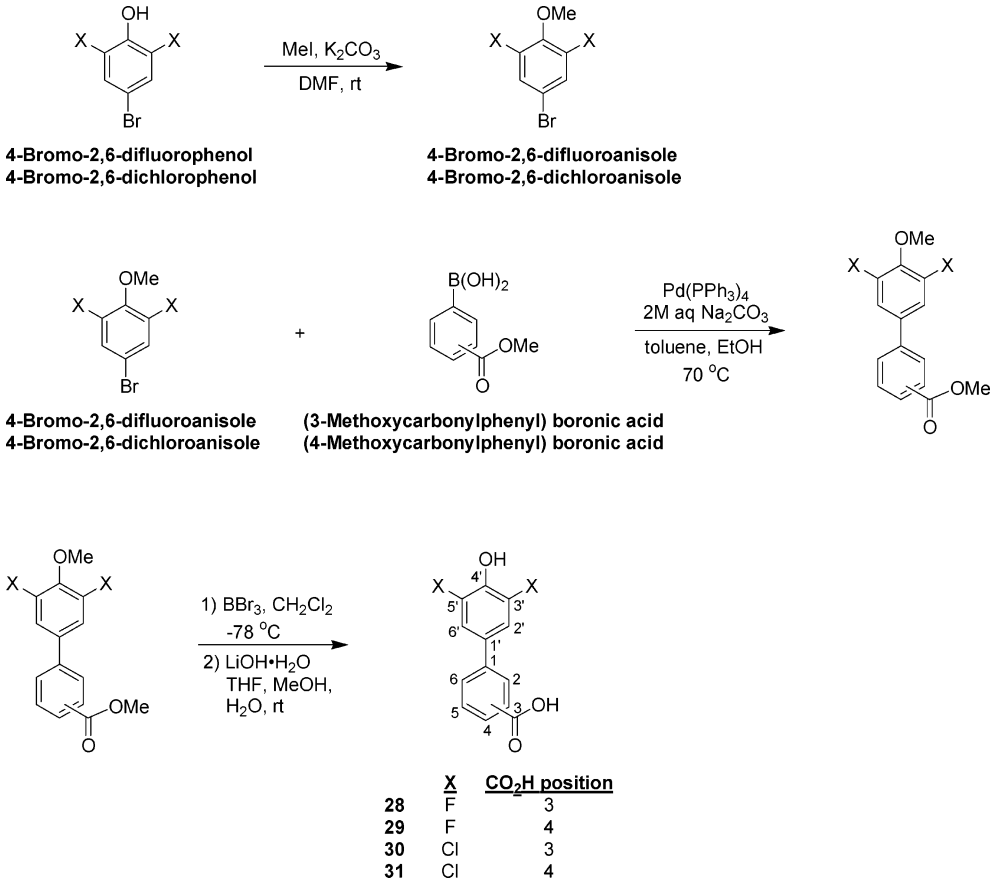

	X	CO_2H position
28	F	3
29	F	4
30	Cl	3
31	Cl	4

Scheme 6. Synthesis of Protected Diflunisal Derivatives

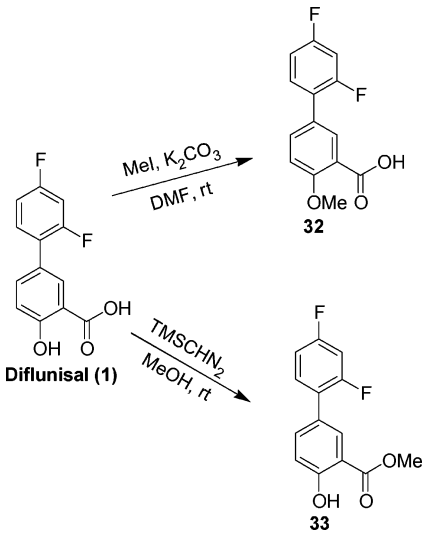

Scheme 7. Synthesis of Halogenated Biphenyls

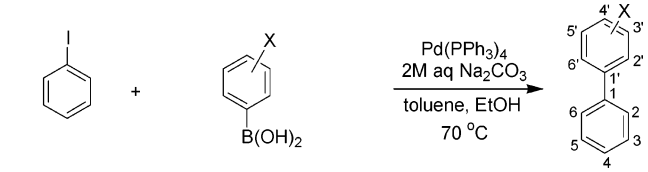

			X
Iodobenzene	2,4-Difluorophenylboronic acid	**34**	2′,4′-F
	4-Fluorophenylboronic acid	**35**	4′-F
	2-Fluorophenylboronic acid	**36**	2′-F
	3,5-Difluorophenylboronic acid	**37**	3′,5′-F
	3,5-Dichlorophenylboronic acid	**38**	3′,5′-Cl

liberated from the resin with 100 mM triethylamine (pH 11.5), and the stoichiometry of small molecule present relative to TTR was determined by reverse-phase HPLC analysis.[41] A maximum of 2 equiv of small molecule may be bound per TTR tetramer. The postwash plasma binding stoichiometries, representing lower limits owing to wash-associated losses, are summarized in Table 1.

Crystal Structures of Inhibitors Bound to TTR. High-resolution X-ray cocrystal structures of **1** and three of its analogues **26**, **18**, and **20** bound to TTR were obtained by soaking TTR crystals with a 10-fold molar excess of inhibitor for more than three weeks (Figure 3).

Diflunisal Bound to TTR. Diflunisal (**1**) binds to TTR in both forward (Figure 3A) and reverse (Figure 3B) modes. In each hormone-binding site of TTR, four different binding conformations of diflunisal were found with approximately equal occupancy—a forward and reverse binding mode each with two symmetrically equivalent binding modes. The biaryl system of diflunisal was shifted away from the center of the hormone binding pocket and occupies two distinct positions to form a 'V' shaped cone of electron density in the hormone-binding pocket of TTR (Figure 3). This mode of binding enhances both hydrophobic and van der Waals interactions between the inhibitor and the hydrophobic pocket of TTR formed by Leu17, Ala 108, Leu 110, Thr 119, and Val 121. The reverse binding mode of diflunisal was augmented by electrostatic interactions between its carboxyl group and the side chain oxygen

Scheme 8. Synthesis of Chlorine-Containing Biphenyls

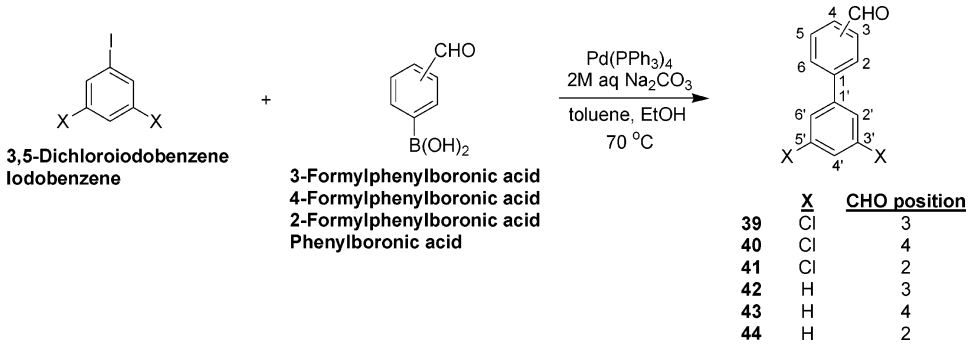

	X	CHO position
39	Cl	3
40	Cl	4
41	Cl	2
42	H	3
43	H	4
44	H	2

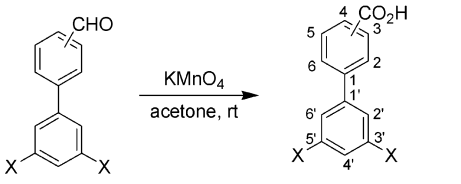

	X	CO_2H position
45	Cl	3
46	Cl	4
47	Cl	2

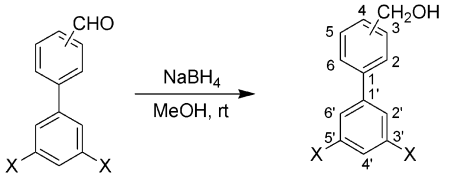

	X	CO_2H position
48	Cl	3
49	Cl	4
50	Cl	2
51	H	3
52	H	4
53	H	2

Scheme 9. Synthesis of 3′,5′-Difluoroformyl-Containing Biphenyls

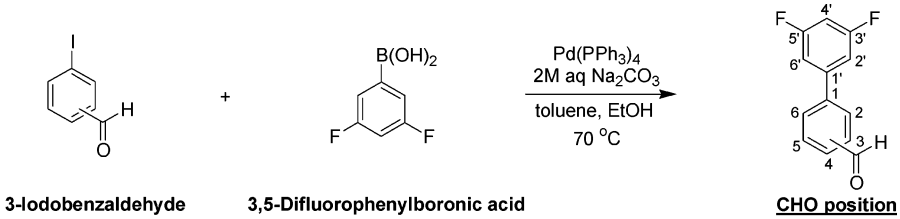

	CHO position
54	3
55	4

of Thr 119 and the main chain oxygen of Ala 108 in the inner binding pocket. Surprisingly Ser 117 neither takes up multiple conformations nor forms any electrostatic interactions with the inhibitor. In the forward mode of binding, one of the fluorine substituents of diflunisal was within hydrogen bonding distance from the Thr 119 side chain oxygen (3.3 Å). In the outer binding pocket, the electron density for the side chain atoms of Lys 15′ was visible only at low σ level indicating it may be in more than one conformation, Figure 3A. The best possible conformation for the Lys 15 residue was modeled at a hydrogen bonding distance from the carboxyl group of diflunisal in the forward binding mode.

Compound 20 Bound to TTR. Compound **20** binds to TTR in the forward binding mode, with the carboxylate-substituted hydrophilic ring oriented in the outer binding pocket to interact electrostatically with Lys 15 and 15′, Figure 3C. The fluorinated aryl ring is positioned in the inner binding pocket wherein the halogens are placed in HBP 2 and 2′. Interestingly, close inspection of both binding sites reveals a significant difference in the orientation of the biphenyl rings. The angles between the planes of the phenyl rings vary from 32 degrees in one binding site to 63 degrees in the other (C.1 vs C.2). This observation may be a result of the negatively cooperative binding of **20** with TTR.

Compound 18 Bound to TTR. Compound **18** binds to TTR in the reverse mode with the carboxylate-substituted hydrophilic aryl ring oriented into the inner pocket, within hydrogen bonding distance of Ser 117 and Ser 117′, Figure 3E. The aryl rings are rotated 34° with respect to one another to take advantage of hydrophobic interactions with Leu 17, Ala 108, Val 121, and Thr 119. The fluorines are positioned in halogen binding pockets

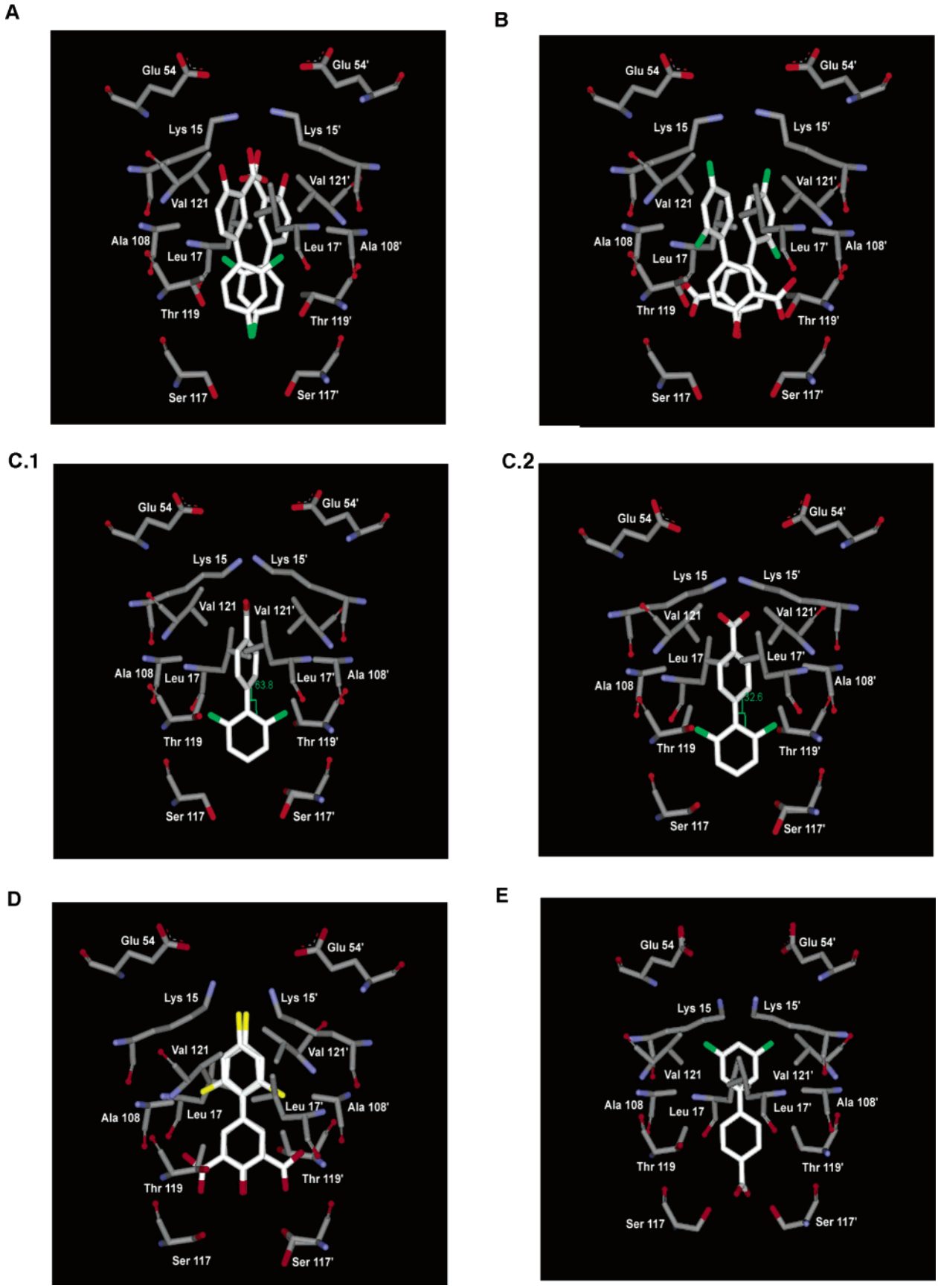

Figure 3. X-ray crystal structures of inhibitors bound to TTR. Diflunisal is shown bound to TTR in the forward binding mode (A) and in the reverse binding mode (B). Inhibitor **20** binds to TTR in the forward binding mode (C) with two observed binding conformations (C.1 and C.2) possessing slightly different angles between the phenyl rings. Inhibitor **26** binds to TTR in the reverse binding mode (D), and the diflunisal analogue **18** also binds in the reverse mode (E). Each figure shows the important residues involved in binding of the small molecule to TTR.

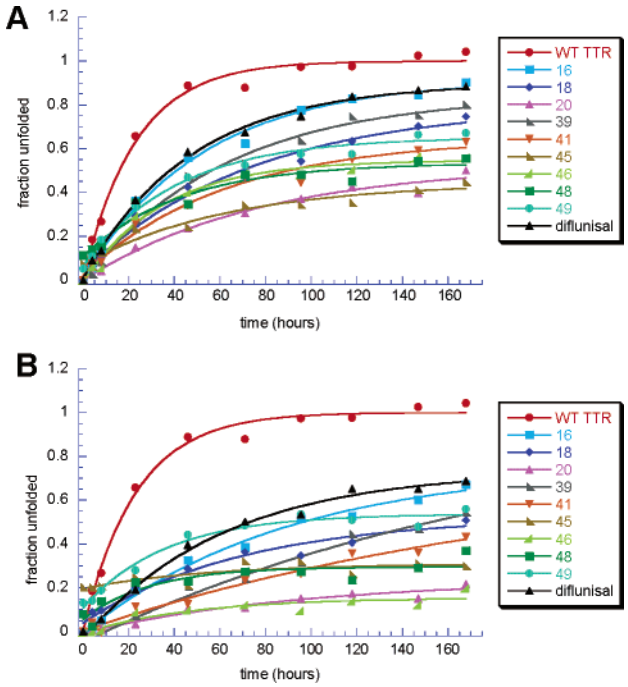

Figure 4. WT TTR (3.6 μM) tetramer dissociation (6.5 M urea) in the presence of 3.6 μM inhibitor (A) and 7.2 μM inhibitor (B).

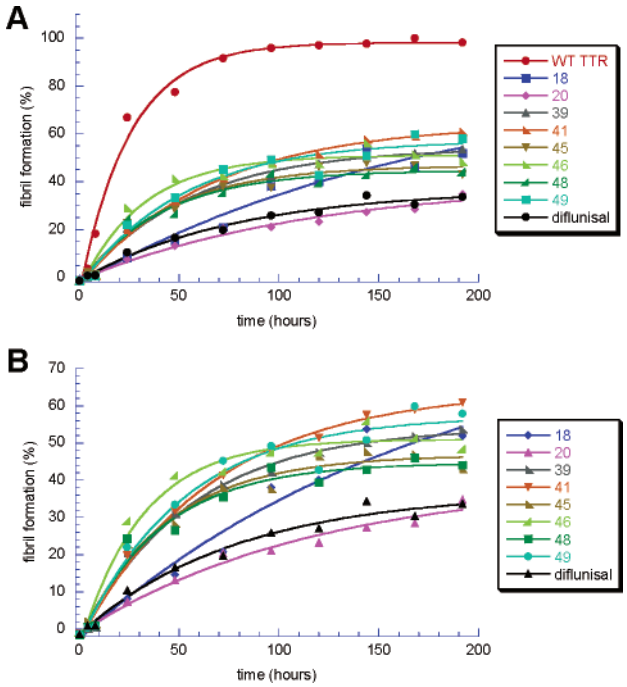

Figure 5. WT TTR (3.6 μM) fibril formation (pH 4.4) in the presence of 3.6 μM inhibitors shown plotted with WT TTR control (A) and plotted without the WT TTR control (B).

1 and 1′. The reverse binding mode was not expected; instead, the carboxylate was envisioned to be positioned in the outer pocket to take advantage of electrostatic interactions with Lys 15 and 15′, with the fluorines sequestered into halogen binding pockets 3 and 3′. However, the reverse binding mode was not a total surprise, as it was observed previously for diclofenac (a biarylamine) and several diclofenac analogues.[24]

Compound 26 Bound to TTR. Substitution of chlorines in place of fluorines in diflunisal induces significant differences in the binding of **26** to TTR. Compound **26** binds to TTR in the reverse binding mode with the carboxyl-substituted aryl ring oriented in the inner binding pocket and chlorines sequestered into halogen binding pockets 2 and 2′ Figure 3D. The residues Ala 108, Lys15, Leu 17, Leu 110, Lys 17, and Thr 119 of TTR protomers forms van der Waals and hydrophobic interactions with the inhibitor. In the inner binding pocket, the side chain of Ser 117 exists in two conformations to interact with the carboxyl substituent of **26** and Ser 117 of the other monomers. The carboxyl group of **26** forms a hydrogen bond with the main chain oxygen of Ala 108. In contrast to diflunisal, the Thr 119 residue orients away from the inhibitor, contributing to the hydrophobicity of the binding pocket rather than hydrogen bonding with the inhibitor.

Rate of TTR Tetramer Dissociation as a Function of Small Molecule Inhibitor Concentration. To further probe the mechanism of action of these small molecules, their ability to stabilize TTR against urea-induced dissociation as a function of time was evaluated. The rate of tetramer dissociation was linked irreversibly to fast, easily monitored, monomer unfolding, employing urea concentrations exceeding those that enable monomer refolding.[43] Unfolding-monitored dissociation was probed by far-UV CD in 6.5 M urea revealing that all the good inhibitiors of acid-mediated amyloidogenesis slowed the rate of tetramer dissociation in a dose-dependent fashion (Figure 4). Several small molecules, including **20**, **46**, and **48**, show a dramatic effect on dissociation of the TTR tetramer, the rate-limiting step of amyloidogenesis.[25]

Rate of TTR Fibril Formation as a Function of Inhibitor Concentration. Since the mode of inhibition of TTR fibril formation by these compounds is suspected to be dose-dependent tuning of the tetramer dissociation barrier through ground-state stabilization, the best inhibitors should slow tetramer dissociation the most.[25] The rate of fibril formation was monitored by turbidity at a final pH of 4.4 over 192 h (Figures 5 and 6). Small molecules possessing the ability to stabilize tetrameric TTR at low pH will prevent tetramer dissociation, misfolding, and misassembly into amyloid. As expected, the best inhibitors of amyloid fibril formation are those that slow tetramer dissociation the most (Figure 4); however, the correlation is not perfect, as some inhibitors bind better in urea than in acidic conditions and vice versa, an observation made earlier with other inhibitors as well.[25]

Analytical Ultracentrifugation. To ensure that the small molecules are stabilizing the tetrameric form of TTR (3.6 μM), equilibrium and velocity analytical ultracentrifugation studies were performed. The quaternary structure of the protein after 72 h incubation with **18** and **20** (3.6 μM or 7.2 μM) at pH 4.4 was determined. The tetramer was the dominant species, both at 3.6 μM and 7.2 μM inhibitor concentration in equilibrium AUC as well as in velocity studies.

Determination of Binding Constants for 18 and 20. Isothermal titration calorimetry was employed to determine the binding constants of **18** and **20** to TTR at pH 8.0 (25 °C) as described previously.[24] Diflunisal and the two analogues bind to TTR with negative cooperativity, a characteristic displayed by many other ligands. Binding at the first site is 15 times stronger

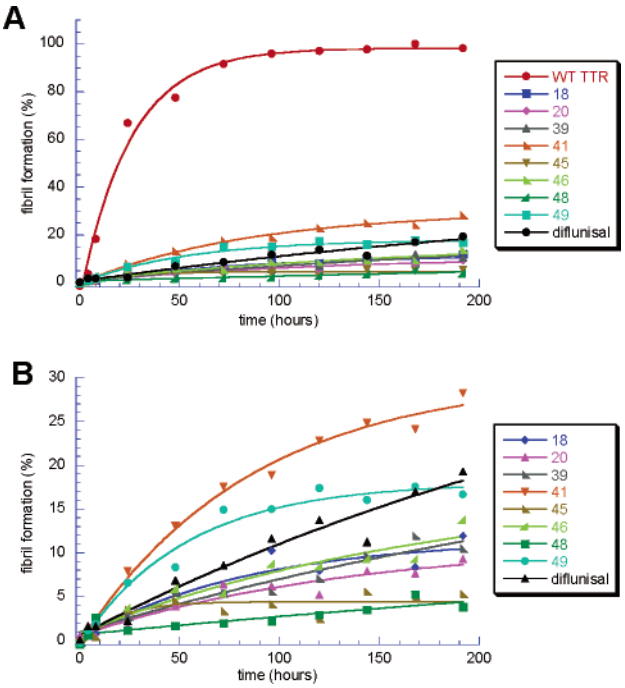

Figure 6. WT TTR (3.6 μM) fibril formation (pH 4.4) in the presence of 7.2 μM inhibitors shown plotted with WT TTR control (A) and plotted without the WT TTR control (B).

Table 2. The First and Second Dissociation Constants for the Binding of **1**, **18**, and **20** to WT TTR Determined by Isothermal Titration Calorimetry (25 °C, pH 8.0). The Binding Constants for **1** Were Reported Previously[25] and Are Provided Here for Comparison Purposes

inhibitor	K_{d1}, nM	K_{d2}, nM
1[a]	75[a]	1100[a]
18	9	1100
20	80	1300

[a] This binding constant was determined previously[25] and is reported here for comparison purposes.

than binding at the second site in the case of diflunisal[25] (**1**) and **20**. Biaryl **18** possesses a K_{d1} approximately 120 times lower than K_{d2} (Table 2).

Discussion

Structure−Activity Relationships and Fibril Formation. On the basis of the inhibitor efficacy data for compounds **2**−**55** (7.2 μM small molecule; 3.6 μM TTR), it is clear that a carboxylate-substituted hydrophilic ring directly connected to a di-halogen functionalized hydrophobic ring is sufficient for excellent activity, Table 1. A phenolic substituent in lieu of a carboxylate (**2**−**10**) yields considerably less active inhibitors, far inferior to the parent compound **1**. Inhibitors with halogens in the ortho or meta position of the hydrophobic ring are superior to compounds lacking halogens or with one para halogen, suggesting that the para halogens do not compliment the HBPs in the same manner as meta and ortho halogenated biaryls. Complete removal of all halogens results in a poor inhibitor, most likely due to the lack of steric complimentarity to fill the halogen binding pockets (**10**, **21**−**22**, **27**, **42**−**44**, **51**−**53**). The best phenolic compound (**8**) is still inferior to **1**, which bears both a phenolic and carboxylate functionality on the hydrophilic ring. Biaryls substituted with a single carboxylate (**11**−**22**) yield excellent amyloid fibril inhibitors **11**, **12**, **15**−**20**, rivaling diflunisal, the exception being small molecules containing only a para halogen (**13** and **14**). A meta- or para-substituted aryl carboxylate is sufficient for endowing excellent inhibition properties, suggesting that the hydroxyl substituent in **1** is not required for good inhibitor activity. In addition, para carboxylate positioning appears to afford superior inhibitors, suggesting that a para carboxylate is better able to take advantage of electrostatic interactions with the ϵ-ammonium groups of Lys 15 and 15′ (forward binding mode), as in the case of **20**, or hydrogen bonding interactions with the Ser 117 and 117′ hydroxyl groups (reverse binding mode) as in the case of **18**, Figure 3E. Biaryls wherein the hydrophobic ring is substituted with halogens in positions other than the para position and the hydrophilic ring with meta and particularly para carboxylates yield highly efficacious TTR amyloid fibril formation inhibitors.

Addition of a hydroxyl subtituent to the ring containing a carboxylate substituent (the salicylic acid substitution **23**−**27**) also results in inhibitors with high activity similar to diflunisal. In biaryls with the salicylic acid core, the exact positioning of the halogens does not appear to be as vital as in the previous cases, suggesting that this ring contributes disproportionately to the binding energy. The para hydroxyl may participate in hydrogen bonding with the ϵ-ammonium groups of Lys 15 and 15′ (forward binding mode) or with the Ser 117 and 117′ hydroxyls (reverse binding mode). Substitution of fluorine in **1** with chlorine (**26**) results in an inhibitor with equal or superior activity, whereas complete removal of the halogens (**27**) results in a modest inhibitor. It should be noted that **27** is only slightly superior to a para carboxylate **22** in vitro, and both are superior to the halogen-free inhibitors with the carboxylate in the meta position, **21**, and the hydroxyl-containing analogue **10**.

Inclusion of a 3′,5′-dihalo-4′-hydroxyl substituent on the halogen-containing ring, with carboxylates in either the para or meta positions (**28**−**31**) results in high inhibitory activity, similar to diflunisal. The 4-hydroxyl substitution was included to more closely mimic the protein's natural ligand, thyroxine. These inhibitors may also more closely mimic the hormone activity of thyroxine and therefore may prove to be thyroid agonists or antagonists, which is undesirable.

Protection of the carboxylate as a methyl ester or the hydroxyl as a methyl ether (**32** and **33**) results in inferior inhibitors compared to **1**. A combination of the loss of charge and the increase in steric bulk probably explains these observations. Removal of all hydrophilic substituents (**34**−**38**), results in poor inhibitors. The biaryl substrate containing only meta chlorine substitution (**38**) is a modest inhibitor, suggesting that the chlorines make enhanced contacts in the halogen binding pockets as compared to fluorine-containing biaryls (**37**).

Several chlorine-containing inhibitors were synthesized and their TTR fibril inhibition activity evaluated. This class of inhibitors containing carboxylates in the meta or para positions (**45** and **46**) possessed high activity, while ortho substitution (**47**) resulted in inferior inhibitors, suggesting that the carboxylate is too far

from the Lys 15 and 15′ ϵ-ammonium groups to make favorable electrostatic interactions (forward binding mode) or from the Ser 117 and 117′ hydroxyl groups to undergo hydrogen bonding interactions (reverse binding mode). Benzylic alcohols **48**−**50** surprisingly proved to be excellent inhibitors of fibril formation. The meta dichloro substitution on one ring is nicely complemented by benzyl alcohol functionality in either the ortho, meta, or para position, potentially due to the hydrogen bonding or water-mediated hydrogen bonding. A series of aldehyde analogues (**39**−**41**) where the CH_2OH groups were replaced by an aldehyde functionality, show good inhibition except in the case of the para aldehyde **41**, possibly owing to hydration of the aldehyde to a gem diol. It is possible that the aldehydes, the benzylic alcohols and the carboxylates bind in the pocket via a different mechanism; however, in the absence of structural information, we cannot rule out a similar binding mode. It is also possible that the aldehydes bind covalently either to Ser 117 (117′) via a hemiacetal or to Lys 15 (15′) via an imine bond. It is interesting to note that substitution of the chlorines with fluorines (**54** and **55**) in the case of the aldehydes results in rather poor inhibitors (**39** and **41**). As before, complete removal of the halogens results in inhibitors with poor activity (**42** and **44**), except in the case of the meta aldehyde **43** where the activity is modest. This modest activity may result from a high degree of hydration. It is surprising that the 3′,5′-difluoro-meta aldehyde (**54**), is inferior to the aldehyde lacking halogens (**42**).

Plasma Selectivity Binding of Inhibitors to TTR. All inhibitors (7.2 μM) that reduce TTR fibril formation (3.6 μM TTR, pH 4.4) to less than 15% of WT TTR amyloidogenesis were tested for their ability to selectively bind to TTR in human plasma in the presence of all of the other plasma proteins including albumin and thyroid binding globulin, Table 1.[41,44] Chlorine-containing biphenyls were selective for binding TTR in human blood plasma (average stoichiometry of 0.8, with a theoretical maximum stoichiometry of 2.0). The average stoichiometry observed was 0.4 for all inhibitors tested. Of the fluorine-containing inhibitors, **18** and **20** exhibited very good and acceptable binding selectivity for TTR, respectively, superior to the 0.13 stoichiometry displayed by **1** under similar conditions. The stoichiometry values reported in Table 1 represent a lower limit due to wash-associated losses of the small molecule from TTR sequestered on a polyclonal antibody resin. Caution should be exercised when interpreting the TTR binding selectivity of **39** and **41**, as these compounds may be covalently attached to TTR.

When inhibitors exhibit excellent TTR amyloid fibril inhibition data in vitro, yet display poor plasma selectivity, it is assumed that they prefer to bind to the drug-binding sites in albumin and/or similar sites in other proteins found in plasma, making it unlikely that such inhibitors will prevent TTR misfolding and amyloidosis in a complex environment like that of blood plasma or CSF.

Select Inhibitors Dramatically slow TTR Tetramer Dissociation Required for Amyloidosis. Tetrameric WT TTR dissociates with a $t_{1/2}$ of 42 h and unfolds 500 000 times faster.[45] Hence, its rate of dissociation can be probed by linking it to unfolding, which is irreversible in 6.5 M urea.[43] Since tetramer dissociation is rate-limiting for amyloidogenesis, all inhibitors displaying excellent in vitro activity and plasma binding stoichiometry exceeding 0.50 should slow tetramer dissociation if the presumed mechanism of action, kinetic stabilization by selective binding to the native state, is correct, Figure 4.

TTR tetramer dissociation rates were measured as a function of inhibitor concentration over a 168 h time-course in 6.5 M urea. Select small molecule inhibitors, specifically **18**, **20**, **39**, **41**, **45**, **46**, **48**, and **49** demonstrate an overall reduction in the extent of tetramer dissociation over 160 h as reflected in the amplitude changes relative to TTR without inhibitor. The rate of tetramer dissociation is also dramatically slowed in the presence of inhibitor, as reflected in the decrease in the slope of the time course. Small molecule inhibitors **20**, **45**, **46**, and **48** are superior, presumably because the inhibitor dissociates very slowly from TTR·I and TTR·I_2 due to their high binding affinity in urea. The formation of TTR·I and TTR·I_2 significantly stabilizes the native state due to their low K_ds, raising the kinetic barrier for tetramer dissociation, substantially in the case of **20**, **45**, **46**, and **48**.[25] Even though **16** and **18** bind to TTR, it is clear that the affinity, and hence the stabilization, is insufficient to affect kinetic stabilization.[25] It is likely significant that the rank ordering of inhibitor efficacy in urea at an inhibitor concentraion of 3.6 μM (3.6 μM protein) is **20** $\approx$ **45** > **46** $\approx$ **48**, which is different than an inhibitor concentration of 7.2 μM (**20** $\approx$ **46** > **45** $\approx$ **48**). This likely reflects a difference in the K_{d2} values in urea.

Kinetic stabilization of the native state is an attractive strategy due to the emerging evidence that misfolded oligomers on or off the amyloid pathway are neurotoxic.[46−50] Achieving kinetic stabilization with small molecule inhibitors allows for a noninvasive treatment for SSA, FAP, and FAC.[25]

Small Molecule Inhibitors Slow TTR Amyloidosis at Low pH. Tetramer dissociation rates in urea in the presence of a given inhibitor do not always predict the ability of the small molecule inhibitor to prevent amyloidosis at low pH,[25] nor should they necessarily since binding constants can vary with environment. Since it is not yet clear how and where amyloid forms in a human, we seek TTR tetramer stabilizers that function well in a variety of denaturing environments. The rate of TTR fibril formation as a function of inhibitor concentration was explored under acidic conditions (pH 4.4), Figures 5 and 6. Inhibitors **20**, **45**, and **48** perform exceptionally well in this environment as well. Inhibitor **46** is a better tetramer stabilizer in urea than in acid, whereas **1** is much better in acid than in urea. The free energy of stabilization associated with the formation of the TTR·I and TTR·I_2 complexes in a given environment determines the extent of ground-state stabilization and associated increase in activation free energy for tetramer dissociation.[25] These data suggest that the small molecules slow TTR amyloidosis at low pH much more efficiently than they slow TTR tetramer dissociation in 6.5 M urea. This is not surprising since amyloidogenesis requires concentration-dependent reassembly after dissociation. The better small molecules are capable of keeping the concentration of

the monomeric amyloidogenic intermediate of TTR at low enough levels to make fibril formation very inefficient.[25] As observed in the urea denaturation of TTR in the presence of small molecules, the rank ordering of inhibitor efficacy at low pH differs significantly from 3.6 μM inhibitor (Figure 5) to 7.2 μM inhibitor concentration (Figure 6). This observation likely reflects the differences in K_{d2} values of each of the inhibitors at low pH. The most dramatic example is that of diflunisal—one of the most efficacious inhibitors of fibril formation at 3.6 μM, but one of the least efficacious at 7.2 μM, owing to its relatively high K_{d2}.

Comparison of Diflunisal Analogues with Diclofenac Analogues. The diflunisal analogues represent a promising class of compounds for the treatment of TTR amyloidosis. While several of the diclofenac analogues studied previously were very good inhibitors of fibril formation,[24] the diflunisal analogues offer an additional class of highly effective TTR tetramer stabilizers. Several of the diclofenac analogues do offer the ability to inhibit fibril formation resulting from the dissociation and misfolding of two TTR mutants—Val30Met and Leu55Pro.[24] The X-ray cocrystal structures demonstrate that the diclofenac analogues primarily bind in the reverse binding mode, however, minor perturbations in the structures of the diflunisal analogues allow for either forward or reverse binding. In addition, diflunisal is able to bind either in the forward or the reverse binding mode, with almost equal occupancy in both modes. The dissociation constants obtained for diclofenac (60 nM for K_{d1} and 1200 nM for K_{d2})[24] were comparable to those obtained for diflunisal and **20**, with **18** demonstrating nearly 10-fold tighter binding for the first binding event as illustrated by its K_{d1} value. In addition, both inhibitor classes displayed negatively cooperative binding. Most remarkably, several diflunisal analogues were very selective for TTR in human blood plasma, offering the potential for decreased toxicity and side-effects.

Outlook for Diflunisal Analogues as a Treatment for TTR Amyloidosis. Twenty eight of the compounds synthesized inhibited TTR amyloidogenesis substantially. Of those, several showed binding stoichiometry exceeding 0.50 equiv in human blood plasma. Both the chlorinated and fluorinated aryl substructures of the better inhibitors are found in known drugs; therefore, there is good reason to believe that these compounds or their analogues could be evolved into drugs not displaying the NSAID activity of **1**, which may prove useful. The fluorinated compounds **18** and **20** bind to and stabilize tetrameric TTR in 6.5 M urea, dramatically slowing the rate of dissociation of the TTR tetramer-the first step of misfolding and amyloidogenesis. These molecules, and others, also dramatically slow acid-mediated TTR amyloidogenesis. Compounds **18**, **20**, **39**, **41**, **45**, **46**, **48**, and **49** perform best at stabilizing the TTR tetramer in urea and under acidic conditions. These biaryls appear to increase the activation barrier associated with tetramer dissociation, the rate-limiting step for amyloid formation, by ground-state stabilization.[25]

Experimental Section

Reagents and solvents were purchased from Aldrich, Lancaster, Acros, Combi-Blocks, Matrix, and Pfaltz-Bauer. THF and CH_2Cl_2 were dried by passage over Al_2O_3. Other solvents and reagents were obtained from commercial suppliers and were used without further purification unless otherwise noted. Reactions were monitored by analytical thin-layer chromatography (TLC) on silica gel 60 F_{254} precoated plates with fluorescent indicator purchased from EM Science. Visualization of the TLC plates was accomplished by UV illumination, phosphomolybdic acid treatment followed by heat, or ceric ammonium molybdate treatment followed by heat. Flash chromatography was performed using silica gel 60 (230−400 mesh) from EM Science. The purity of new compounds that were essential to the conclusions drawn in the text were determined by HPLC. Normal phase HPLC was performed with a Waters 600 pump/controller, a Waters 996 photodiode array detector, and a Waters NovaPak silica column. The solvent system employed was hexanes and ethyl acetate, and gradients were run from 50:50 hexanes:ethyl acetate to 0:100 hexanes:ethyl acetate over 30 min. Reverse phase HPLC was performed with a Waters 600 pump/controller, a Waters 2487 dual wavelength detector and a Vydac protein and peptide C18 column. Solvent system A was 95:5 water:acetonitrile with 0.5% trifluoroacetic acid and solvent B was 5:95 water: acetonitrile with 0.5% trifluoroacetic acid. Gradients were run from 100:0 A:B to 0:100 A:B over 20 min with a hold at 100% B for an additional 10 min. Circular dichroism spectroscopy was performed on an AVIV Instruments spectrometer, model 202SF. NMR spectra were recorded on a Varian FT NMR spectrometer at a proton frequency of 400 MHz. Proton chemical shifts are reported in parts per million (ppm) with reference to $CHCl_3$ as the internal chemical shift standard (7.26 ppm) unless otherwise noted. Coupling constants are reported in hertz (Hz). Carbon chemical shifts are reported in parts per million (ppm) with reference to $CDCl_3$ as the chemical shift standard (77.23 ppm) unless otherwise noted. All mass spectra were obtained at The Scripps Research Institute Center for Mass Spectrometry or the University of Illinois Mass Spectrometry Laboratory.

Fibril Formation Assay. Each compound was subjected to a stagnant fibril formation assay as described previously.[12,18,24] Compounds were dried over P_2O_5 overnight and dissolved in DMSO to a final concentration of 7.2 mM to provide a primary stock solution (10× stock). A secondary stock solution was prepared by 5-fold dilution of the primary stock solution with DMSO to a final concentration of 1.44 mM (2× stock). The acid-mediated amyloidogenicity of TTR (3.6 μM) in the presence of small molecules (1.44 mM) was performed as follows: To a disposable UV cuvette were added 495 μL of a 0.4 mg/mL WT TTR protein solution in 10 mM sodium phosphate, 100 mM KCl. and 1 mM EDTA (pH 7.6) and 5 μL of the 1.44 mM secondary stock inhibitor solution in DMSO (2× stock). The mixture was vortexed and incubated for 30 min (25 °C), at which time the pH was lowered to 4.4 with 500 μL of 200 mM acetate, 100 mM KCl, and 1 mM EDTA (pH 4.2). The final 1 mL solution was vortexed and incubated for 72 h at 37 °C without agitation. After 72 h, the cuvettes were vortexed to suspend any fibrils present, and the turbidity of the suspension was measured at 350 and 400 nM using a UV−Vis spectrometer. The percent fibril formation was obtained by the ratio of the observed turbidities for each TTR plus inhibitor sample relative to that of a sample prepared the same way, but lacking small molecule inhibitor multiplied by 100. The fibril formation assay employing equimolar small molecule and TTR concentrations (3.6 μM) was performed as above using a 1× secondary stock solution. The 1× stock solution was prepared by 10-fold dilution of the 7.2 mM 10× primary stock solution with DMSO to a final concentration of 0.72 mM and used in the fibril formation assay as described above. All assays were performed in triplicate and all compounds were assayed using wild-type TTR. All compounds were found to be soluble throughout the course of the experiment by testing the turbidities of the solutions in the absence of WT TTR, ensuring that turbidity was the result of TTR amyloid formation.

Table 3. X-ray Crystallographic Data for Compounds **1**, **18**, **20**, and **26**

	TTR·**1**	TTR·**18**	TTR·**20**	TTR·**26**
resolution (Å)	35.58−1.85	42.18−1.50	64.5−1.7	51.30−1.7
no. of unique reflections	20 478	33 741	25 634	25 486
completeness (%) (overall/outer shell)	98.4/99.0	95.0/98.0	98.0/99.0	99.0/98.0
R_{sym} (overall/outer shell)	0.09/0.31	0.03/0.32	0.08/0.39	0.07/0.40
	Refinement			
resolution (Å)	35.58−1.85	42.18−1.54	64.5−1.7	51.30−1.7
R-factor/*R*-free (%)	21.2/23.6	22.2/24.5	22.5/24.0	21.5/24.2
rmsd bond length (Å)	0.03	0.06	0.02	0.02
rmsd bond angles (deg)	2.3	2.7	1.9	1.9

Plasma Selectivity Assay.[41] The binding stoichiometries of potential inhibitors to TTR in blood plasma were evaluated by an antibody capture/HPLC method as previously described.[41] A 1.5-mL eppendorf tube was filled with 1.0 mL of human blood plasma and 7.5 μL of a 1.44 mM DMSO solution of the small molecule under evaluation. The solution was incubated and gently rocked at 37 °C for 24 h. A 1:1 gel:TSA (Tris saline) slurry (125 μL) of quenched sepharose[41] was added to the solution and gently rocked at 4 °C for 1 h. The solution was centrifuged (16 000 × g) and the supernatant was divided into two 400 μL aliquots, which were then added to different 200 μL samples of a 1:1 gel:TSA slurry of the anti-TTR antibody-conjugated sepharose. The solutions were gently rocked at 4 °C for 20 min and centrifuged (16 000 × g), and the supernatant was removed. The gel was washed with 1 mL of TSA/0.05% saponin (3×, 10 min each) at 4 °C, followed by 1 mL of TSA (2×, 10 min each) at 4 °C. The samples were centrifuged (16 000 × g), the final wash was removed, and 155 μL of 100 mM triethylamine, pH 11.5, was added to elute the TTR and bound small molecules from the antibodies. After gentle rocking at 4 °C for 30 min, the elution sample was centrifuged (16 000 × g) and 145 μL of the supernatant, containing TTR and inhibitor, was removed. The supernatant was then analyzed by reverse-phase HPLC as described previously.[41]

Crystallization and X-ray Data Collection. Crystals of WT TTR were obtained from protein solutions at 7 mg/mL (in 100 mM KCl, 1 mM EDTA, 10 mM sodium phosphate, pH 7.0, 0.35−0.50 M ammonium sulfate) equilibrated against 2 M ammonium sulfate in hanging drop experiments. The TTR−ligand complexes were prepared from crystals soaked for more than three weeks with a 10-fold molar excess of the ligand. A CCD-PXL-L600 detector (Bruker instruments) coupled to an RU200 rotating anode X-ray generator was used for data collection of **20** and **26**. The Quantum-4 detector at the monochromatic high-energy source of 14-BM-C, BIOCARS, Advance Photon Source, was used for the data collection of diflunisal and **18**. The crystals were placed in paratone oil as a cryoprotectant and cooled for diffraction experiments (120 K for **20** and **26**, and 100 K for **1** and **18**). Crystals of TTR· ligand complex structures are isomorphous with the apo crystal form with unit cell dimensions close to $a = 43$ Å, $b = 85$ Å, and $c = 66$ Å; space group $P2_12_12$ with two monomers in the asymmetric unit. Data sets of **1** and **18** were reduced with DENZO and SCALEPAC.[51] Data sets of **20** and **26** were reduced with SAINT and PROSCALE (Bruker AXS, Inc.).

Structure Determination and Refinement. The protein atomic coordinates for TTR from the Protein Data Bank (accession number 1 μ_BZ) were used as a starting model during the molecular replacement search by EPMR.[52] The best solutions from EPMR were refined by molecular dynamics and energy minimization protocols of CNS.[53] The resulting difference Fourier maps revealed binding of the ligands (in two conformations for **18**, **20**, and **26**, and four conformations for **1**) in each binding pocket of the TTR tetramer. Using these maps, the ligand could be unambiguously placed into the density and was included in the crystallographic refinement. After several cycles of simulated annealing and subsequent positional and temperature factor refinement, water molecules were placed into difference Fourier maps. The final cycle of map-fitting was done using the unbiased weighted electron density map calculated by the shake/warp bias removal protocol.[54−56] All binding conformations of the ligand were in good agreement with unbiased annealed omit maps as well as the shake/warp unbiased weighted maps phased in the absence of the inhibitor. Final cycles of the refinement were carried out by the restrained refinement protocol of Refmac.[55,56] Because of the lack of interpretable electron densities in the final map, the nine *N*-terminal and three *C*-terminal residues were not included in the final model. A summary of the crystallographic analysis is presented in Table 3.

Tetramer Dissociation Kinetics Evaluated by Linked Monomer Unfolding in Urea. Slow tetramer dissociation is not detectable by far-UV CD spectroscopy, but is linked to the rapid (500 000-fold faster) unfolding step easily detectable by far-UV CD as described previously.[25] TTR tetramer (3.6 μM) dissociation kinetics as a function of inhibitor (3.6 μM) were evaluated by adding 3.6 μL of a 1 mM solution (in ethanol) of the small molecule of interest to 69 μL of WT TTR (2.90 mg/mL, 10 mM sodium phosphate, 100 mM KCl, 1 mM EDTA, pH 7.0) to which was added 127.4 μL of phosphate buffer. For an inhibitor concentration (7.2 μM) twice that of the TTR concentration (3.6 μM), 7.2 μL of a 1 mM solution (in ethanol) of the small molecule of interest was added to 69 μL of WT TTR (2.90 mg/mL, 10 mM sodium phosphate, 100 mM KCl, 1 mM EDTA, pH 7.0) to which was added 123.8 μL of phosphate buffer. 100 μL of the protein-small molecule solution of interest was added to a solution of 600 μL of 10.3 M urea and 300 μL of phosphate buffer, to yield a final urea concentration of 6.5 M. The solutions were vortexed and the circular dichroism spectra were collected at the following intervals: 0, 5, 8, 23, 46, 71, 95, 118, 144, and 168 h. A control sample containing 7.2 μL of ethanol rather than small molecule was prepared for comparison and the spectra were collected at the time points identified above. CD spectra were collected between 220 and 213 nm, with scanning every 0.5 nm and an averaging time of 10 s. Each wavelength was scanned once. The values for the amplitude were averaged between 220 and 213 nm to determine the extent of β-sheet loss throughout the experiment.

Fibril Formation Time-Course. The rate of acid-mediated fibril formation was followed at pH 4.4 by turbidity as described previously.[25] Compounds were dried over P_2O_5 overnight and dissolved in DMSO to a final concentration of 7.2 mM to provide a primary stock solution (10× stock). A secondary stock solution was prepared by 5-fold DMSO dilution of the primary stock solution to yield a final concentration of 1.44 mM (2× stock). The fibril formation assay employing an inhibitor concentration of 7.2 μM relative to 3.6 μM TTR (tetramer) was performed as follows: To a disposable UV cuvette were added 495 μL of a 0.4 mg/mL WT TTR protein solution in 10 mM sodium phosphate, 100 mM KCl, and 1 mM EDTA (pH 7.6) and 5 μL of the 1.44 mM secondary inhibitor stock solution (2× stock). The mixture was vortexed and incubated for 30 min (25 °C). After 30 min, the pH was lowered to 4.4 with 500 μL of 200 mM acetate, 100 mM KCl, 1 mM EDTA (pH 4.2). The final 1 mL solution was vortexed and incubated at 37 °C without agitation. The solutions were vortexed and turbidity at 350 and 400 nm was measured. UV spectra were collected at the following intervals: 0, 4, 8, 24, 48, 72, 96, 120, 144, 168, and 192 h after acidification. A control sample containing 5 μL of DMSO was prepared for comparison,

and the spectra were collected at the time points above. Each small molecule solution was prepared in groups of 10 to prevent disturbance of the cuvettes before a reading was taken. After a UV absorbance was obtained, the cuvettes corresponding to that time-point were discarded. The fibril formation assay employing equimolar (3.6 μM) TTR and inhibitor concentration was performed as above using a 1× secondary inhibitor stock solution prepared as follows: A stock solution was prepared by 10-fold dilution of the 7.2 mM 10× primary stock solution with DMSO to a final concentration of 0.72 mM and used in the fibril formation assay as described above. All compounds were found to be soluble throughout the course of the experiment, ensuring that turbidity was the result of TTR amyloid formation.

Analysis of TTR Quaternary Structure in the Presence of Inhibitors at pH 4.4. The mechanism by which **18** and **20** stabilize TTR was evaluated by incubating the protein (3.6 μM) for 72 h under the conditions of the stagnant fibril formation assay in the presence of either 3.6 μM or 7.2 μM small molecule. After 72 h, the samples were centrifuged (14 000 × *g*) and the supernatant was removed from any solid that was formed in the assay. Equilibrium and velocity ultracentrifugation analysis was achieved with a Beckman XL-I analytical ultracentrifuge. The acquisition and analysis of data was performed as described previously.[21,24,57,58]

Isothermal Titration Calorimetry. The dissociation constants characterizing the binding of **18** and **20** to WT TTR were determined using a Microcal isothermal titration calorimeter (Microcal Inc., Northhampton, MD). A solution of small molecule (300 μM or 500 μM in 25 mM tris buffer, 100 mM KCl, 1 mM EDTA, 12% EtOH, pH 8.0) was prepared and titrated into an ITC cell containing WT TTR (15 μM or 25 μM in 25 mM tris buffer, 100 mM KCl, 1 mM EDTA, 12% EtOH, pH 8.0). The initial injection of 2.5 μL was followed by 50 injections of 5.0 μL each (25 °C). Integration of the thermogram after subtraction of blanks yielded a binding isotherm that fit best to a model of two sequential binding sites with negative cooperativity. The data were fit by a nonlinear least squares approach with four adjustable parameters, namely, K_1, ΔH_1, K_2, ΔH_2 using the ITC data analysis module in ORIGIN version 2.9 provided by Microcal.[24]

Synthesis and Characterization of Biaryl Inhibitors. Acetic Acid 3-Iodophenyl Ester.[59] Acetic anhydride (4.3 mL, 45.47 mmol) was added to a solution of 3-iodophenol (1.00 g, 4.55 mmol) in pyridine (5 mL). After stirring for 14 h, the reaction was concentrated in vacuo and flash chromatographed (10:1 hexane:ethyl acetate) to yield acetic acid 3-iodophenyl ester (1.16 g, 98%) as a white solid. ^{1}H NMR ($CDCl_3$, 400 MHz) δ 7.58 (dd, 1H, J = 8.9, 2.0, 1.7 Hz), 7.47 (ddd, 1H, J = 2.4, 1.6, 0.4 Hz), 7.09 (m, 2H), 2.29 (s, 3H). ^{13}C NMR ($CDCl_3$, 100 MHz) δ 169.3, 151.2, 135.1, 130.9, 121.3, 93.7, 21.1.

Acetic Acid 4-Iodophenyl Ester.[59] Acetic anhydride (4.3 mL, 45.47 mmol) was added to a solution of 4-iodophenol (1.01 g, 4.55 mmol) in pyridine (5 mL). After stirring for 14 h, the reaction was concentrated in vacuo and flash chromatographed (10:1 hexane:ethyl acetate) to yield acetic acid-4-iodophenyl ester (1.13 g, 95%) as a white solid. ^{1}H NMR ($CDCl_3$, 400 MHz) δ 7.68 (*AA′*XX′, 2H, $J_{AA'} = J_{XX'} = 2.9$ Hz, $J_{XA} = J_{X'A'} = 8.4$ Hz, $J_{X'A} = J_{XA'} = 0.6$ Hz, $\nu_A = \nu_{A'} = 3070.2$ Hz, $\nu_X = \nu_{X'} = 2742.8$ Hz), 6.86 (AA′*XX′*, 2H, as above), 2.29 (s, 1H). ^{13}C NMR ($CDCl_3$, 100 MHz) δ 169.2, 150.6, 138.6, 123.9, 90.0, 21.3.

General Procedure for Pd-Mediated Suzuki Coupling Reactions To Prepare 2, 3, 8, 9. To a solution of the appropriate acetic acid-iodophenyl ester (1.0 equiv) dissolved in enough toluene to give a concentration of 0.05 M was added a solution of phenyl boronic acid (1.1 equiv) dissolved in EtOH to give a 0.6 M solution with respect to the boronic acid. A 2 M aqueous solution of Na_2CO_3 was added to give a final reaction concentration of 0.03 M with respect to the acetic acid-iodophenyl ester, followed by addition of $Pd(PPh_3)_4$ (4.0 mol %). The reaction was heated to reflux under Ar for 20 h and, upon completion, was cooled to room temperature, extracted with CH_2Cl_2 (2×), washed with brine (1×), dried over $MgSO_4$, and concentrated in vacuo. The residue was purified by flash chromatography (10:1 hexane:ethyl acetate) to afford the acetylated biphenyl.

A catalytic amount of Na° was added to a solution of the acetylated biphenyl in MeOH to provide a final reaction concentration of 0.3 M. The reaction was allowed to stir at room temperature under Ar for 12 h, after which Dowex 50W−X8 cation-exchange resin was added to neutralize the reaction mixture. The resin was filtered, and the filtrate was concentrated in vacuo and flash chromatographed (3:1 hexane:ethyl acetate) to afford the hydroxybiphenyl products as white solids in 22−75% yields.

Characterization for 2, 3, 8 and 9.

2′,4′-Difluorobiphenyl-3-ol (2). ^{1}H NMR (DMSO-d_6, 400 MHz) δ 9.63 (br s, 1H), 7.54 (td, 1H, J = 8.9, 6.7 Hz), 7.34 (ddd, 1H, J = 11.1, 9.2, 2.6 Hz), 7.27 (m, 1H), 7.17 (tdd, 1H, J = 8.3, 2.6, 1.2 Hz), 6.92 (m, 2H), 6.81 (ddd, 1H, J = 8.1, 2.5, 1.0 Hz). ^{13}C NMR (DMSO-d_6, 100 MHz) δ 162. 8, 160.3, 157.4, 135.4, 131.8, 129.7, 119.4, 115.6, 114.9, 111.9, 104.4. HRESIMS calculated for $C_{12}H_8F_2O$ (M − H) 205.0466, found 205.0465. Normal phase HPLC retention time: 10.5 min. Reverse phase HPLC retention time: 1.3 min. >99% pure.

2′,4′-Difluorobiphenyl-4-ol (3). ^{1}H NMR (DMSO-d_6, 400 MHz) δ 7.49 (td, 1H, J = 9.4, 8.6 Hz), 7.34 (*AA′*XX′, 2H, $J_{AA'} = J_{XX'} = 2.5$ Hz, $J_{XA} = 8.7$ Hz, $J_{X'A'} = 8.5$ Hz, $J_{X'A} = 0.3$ Hz, $J_{XA'} = 0.3$ Hz, $\nu_A = \nu_{A'} = 2934.1$ Hz, $\nu_X = \nu_{X'} = 2746.2$ Hz), 7.28 (ddd, 2H, J = 11.3, 9.4, 2.6 Hz), 7.13 (dddd, 1H, J = 8.3, 7.5, 2.8, 1.0 Hz), 6.87 (AA′*XX′*, 2H, as above). ^{13}C NMR (DMSO-d_6, 100 MHz) δ 162.3, 160.0, 157.2, 131.4, 129.9, 124.8, 115.4, 111.8, 104.3. HRESIMS calculated for $C_{12}H_8F_2O$ (M − H) 205.0464, found 205.0465. Normal phase HPLC retention time: 11.2 min. Reverse phase HPLC retention time: 12.6 min. >98% pure.

3′,5′-Difluorobiphenyl-3-ol (8). ^{1}H NMR (DMSO-d_6, 400 MHz) δ 9.65 (br s, 1H), 7.34 (m, 2H), 7.28 (t, 1H, J = 7.9 Hz), 7.19 (tt, 1H, J = 9.1, 2.2 Hz), 7.13 (ddd, 1H, J = 7.8, 1.8, 1.0 Hz), 7.08 (t, 1H, J = 2.1 Hz), 6.86 (ddd, 1H, J = 8.0, 2.4, 1.0 Hz). ^{13}C NMR (DMSO-d_6, 100 MHz) δ 162.9, 158.0, 144.1, 139.1, 130.1, 117.6, 115.7, 109.7, 102.6. HRESIMS calculated for $C_{12}H_8F_2O$ (M − H) 205.0465, found 205.0468. Normal phase HPLC retention time: 11.4 min. Reverse phase HPLC retention time: 12.9 min. >99% pure.

3′,5′-Difluorobiphenyl-4-ol (9). ^{1}H NMR ($CDCl_3$, 400 MHz) δ 7.44 (*AA′*XX′, 2H, $J_{AA'} = J_{XX'} = 3.0$ Hz, $J_{XA} = 8.0$ Hz, $J_{X'A'} = 8.5$ Hz, $J_{X'A} = 0.7$ Hz, $J_{XA'} = 0.5$ Hz, $\nu_A = \nu_{A'} = 2973.8$ Hz, $\nu_X = \nu_{X'} = 2766.0$ Hz), 7.05 (dtd, 2H, J = 6.6, 2.4, 0.7 Hz), 6.92 (AA′*XX′*, 2H, as above), 6.74 (tt, 1H, J = 8.9, 2.4 Hz), 5.11 (s, 1H). ^{13}C NMR ($CDCl_3$, 100 MHz) δ 164.7, 156.1, 144.2, 131.8, 128.6, 116.1, 109.6, 102.1. HRESIMS calculated for $C_{13}H_8Cl_2O_2$ (M − H) 205.0465, found 205.0465. Normal phase HPLC retention time: 10.8 min. Reverse phase HPLC retention time: 12.9 min. >99% pure.

2′,4′-Difluorobiphenyl-3-carboxylic Acid (11). 3-Iodobenzoic acid (200 mg, 0.81 mmol), DIEA (140 μL, 0.81 mmol), EDCI·HCl, and HOBt were added to a solution of Wang resin (265 mg, 0.67 mmol, 2.53 mmol/g) swelled in CH_2Cl_2 (10 mL). After rigorous shaking on a peptide shaker for 22 h at room temperature, the solvent was removed and the resin was washed with DMF (3 × 10 mL) and CH_2Cl_2 (3 × 10 mL) and dried thoroughly in vacuo.

2,4-Difluorophenyl boronic acid (112 mg, 0.71 mmol), K_2CO_3 (98 mg, 0.71 mmol), and $Pd_2(dba)_3$ (4 mg, 0.01 mmol) were added to a solution of functionalized Wang resin (140 mg, 0.35 mmol) swelled in DMF (2 mL). After stirring at room temperature, the reaction was filtered and the resin was washed with DMF (3×), H_2O (3×), CH_2Cl_2 (3×), and MeOH (3×) and dried thoroughly in vacuo.

A solution of TFA:CH_2Cl_2 (3 mL 1:1) was added to functionalized resin (140 mg, 0.35 mmol) and shaken vigorously on a peptide shaker for 13 h at room temperature. After completion, the reaction was filtered, the resin was washed with CH_2Cl_2 (3×), and the filtrate was concentrated in vacuo and purified by flash chromatography (2:1 hexane:ethyl acetate, 0.5% acetic acid) to afford **11** (81 mg, 100%) as a white solid. ^{1}H NMR (DMSO-d_6, 400 MHz) δ 13.19 (br s, 1H), 8.07 (q, 1H, J = 1.7

Hz), 7.99 (dt, 1H, J = 7.9, 1.6 Hz), 7.78 (dq, 1H, J = 7.8, 1.3 Hz), 7.64 (m, 2H), 7.40 (ddd, 1H, J = 11.1, 8.8, 2.5 Hz), 7.22 (tdd, 1H, J = 8.4, 2.8, 1.0 Hz). ^{13}C NMR (DMSO-d_6, 100 MHz) δ 167.0, 160.7, 160.4, 134.5, 133.0, 132.0, 131.3, 129.4, 129.1, 128.7, 123.9, 112.2, 104.6. HRESIMS calculated for $C_{13}H_8F_2O_2$ (M − H) 233.0414, found 233.0426. Normal phase HPLC retention time: 13.7 min. Reverse phase HPLC retention time: 12.5 min. >99% pure.

General Procedure for Pd-Mediated Suzuki Coupling Reactions To Prepare 12, 15, 16, 17, 18, 19, 20, 22. To a solution of the appropriate methyl bromobenzoate (1.0 equiv) dissolved in enough toluene to give a concentration of 0.1 M was added a solution of phenyl boronic acid (2.0 equiv) dissolved in EtOH to give a 1.0 M solution of boronic acid. A 2 M aqueous solution of Na_2CO_3 was added to give a final reaction concentration of 0.06 M with respect to the bromobenzoate, followed by addition of $Pd(PPh_3)_4$ (10.0 mol %). The reaction was stirred at 70 °C under Ar for 25 h and, upon completion, was cooled to room temperature, extracted with CH_2Cl_2 (2×), washed with brine (1×), dried over $MgSO_4$, and concentrated in vacuo. The residue was purified by flash chromatography (10:1 hexane:ethyl acetate) to afford the methyl ester.

To a solution of methyl ester (1.0 equiv) in THF:MeOH:H_2O (1:1:1) at a concentration of 0.06 M was added LiOH·H_2O (3.0 equiv). The reaction was stirred at room temperature for 4 h and, upon completion, was acidified with 30% HCl, extracted with ethyl acetate (3 × 5 mL), dried over $MgSO_4$, and concentrated in vacuo. The residue was purified by flash chromatography (CH_2Cl_2, 1% MeOH, 0.2% acetic acid) to afford the biphenyl carboxylic acids as white solids in 6−93% yields.

Characterization for 12, 15, 16, 17, 18, 19, 20, and 22. 2′,4′-Difluorobiphenyl-4-carboxylic Acid (12). ^{1}H NMR (DMSO-d_6, 400 MHz) δ 13.09 (br s, 1H), 8.04 (AA'XX′, 2H, $J_{AA'} = J_{XX'}$ = 2.0 Hz, $J_{XA} = J_{X'A'}$ = 8.0 Hz, $J_{X'A} = J_{XA'}$ = 0.7 Hz, $\nu_A = \nu_{A'}$ = 3213.3 Hz, $\nu_X = \nu_{X'}$ = 3056.2 Hz), 7.65 (AA′XX', 2H, as above), 7.63 (m, 1H), 7.38 (ddd, 1H, J = 11.2, 9.0, 2.8 Hz), 7.21 (td, 1H, J = 8.4, 2.2 Hz). ^{13}C NMR (DMSO-d_6, 100 MHz) δ 167.1, 160.8, 158.0, 138.6, 132.1, 130.1, 129.6, 129.0, 123.9, 112.2, 104.7. HRESIMS calculated for $C_{13}H_8F_2O_2$ (M − H) 233.0414, found 233.0407. Normal phase HPLC retention time: 13.3 min. Reverse phase HPLC retention time: 12.6 min. >99% pure.

2′-Fluorobiphenyl-3-carboxylic Acid (15). ^{1}H NMR (CD_3-OD, 400 MHz) δ 8.18 (q, 1H, J = 1.4 Hz), 8.03 (dt, 1H, J = 7.8, 1.3 Hz), 7.76 (dq, 1H, J = 7.7, 1.5 Hz), 7.55 (t, 1H, J = 7.8 Hz), 7.48 (td, 1H, J = 7.8, 1.7 Hz), 7.38 (dddd, 1H, J = 8.3, 7.5, 5.1, 1.8 Hz), 7.26 (td, 1H, J = 7.6, 1.3 Hz), 7.20 (ddd, 1H, J = 11.0, 8.2, 1.2 Hz). ^{13}C NMR (CD_3OD, 100 MHz) δ 169.7, 161.2, 137.5, 134.6, 132.4, 132.0, 131.3, 130.1, 129.9, 129.5, 126.0, 117.2. HRESIMS calculated for $C_{13}H_9FO_2$ (M − H) 215.0508, found 215.0498. Normal phase HPLC retention time: 10.6 min. Reverse phase HPLC retention time: 12.1 min. >99% pure.

2′-Fluorobiphenyl-4-carboxylic Acid (16). ^{1}H NMR (DMSO-d_6, 400 MHz) δ 13.10 (br s, 1H), 8.05 (AA'XX′, 2H, $J_{AA'} = J_{XX'}$ = 1.7 Hz, $J_{XA} = J_{X'A'}$ = 8.5 Hz, $J_{X'A} = J_{XA'}$ = 0.3 Hz, $\nu_A = \nu_{A'}$ = 3217.9 Hz, $\nu_X = \nu_{X'}$ = 3070.0 Hz), 7.67 (AA′XX', 2H, as above), 7.58 (td, 1H, J = 8.0, 1.8 Hz), 7.34 (m, 1H). ^{13}C NMR (DMSO-d_6, 100 MHz) δ 167.1, 159.1, 139.4, 130.8, 130.3, 130.2, 129.6, 129.0, 127.3, 125.1, 116.2. HRESIMS calculated for $C_{13}H_9FO_2$ (M − H) 215.0508, found 215.0515. Normal phase HPLC retention time: 12.3 min. Reverse phase HPLC retention time: 12.2 min. >99% pure.

3′,5′-Difluorobiphenyl-3-carboxylic Acid (17). ^{1}H NMR (acetone-d_6, 400 MHz) δ 8.30 (td, 1H, J = 2, 0.5 Hz), 8.10 (dtd, 1H, J = 7.6, 1.1, 0.5 Hz), 7.97 (ddd, 1H, J = 7.8, 2.0, 1.1 Hz), 7.64 (td, 1H, J = 7.8, 0.6 Hz), 7.39 (m, 2H), 7.06 (tt, 1H, J = 9.3, 2.4 Hz). ^{13}C NMR (acetone-d_6, 100 MHz) δ 167.4, 165.6, 163.2, 144.6, 139.8, 132.5, 132.4, 130.6, 130.3, 128.9, 111.0, 103.7. HRESIMS calculated for $C_{13}H_8F_2O_2$ (M − H) 233.0414, found 233.0425. Normal phase HPLC retention time: 13.5 min. Reverse phase HPLC retention time: 12.7 min. >99% pure.

3′,5′-Difluorobiphenyl-4-carboxylic Acid (18). ^{1}H NMR (DMSO-d_6, 400 MHz) δ 13.15 (br s, 1H), 8.02 (d, 2H, J = 8.2 Hz), 7.85 (d, 2H, J = 8.5 Hz), 7.49 (m, 2H), 7.26 (tt, 1H, J = 9.4, 2.4 Hz). ^{13}C NMR (DMSO-d_6, 100 MHz) δ 166.4, 164.1, 161.7, 142.6, 141.6, 130.9, 130.0, 127.1, 110.2, 103.5. HRESIMS calculated for $C_{13}H_8F_2O_2$ (M − H) 233.0414, found 233.0423. Normal phase HPLC retention time: 13.0 min. Reverse phase HPLC retention time: 12.8 min. >99% pure.

2′,6′-Difluorobiphenyl-3-carboxylic Acid (19). ^{1}H NMR (DMSO-d_6, 400 MHz) δ 8.03 (dt, 1H, J = 7.8, 1.6 Hz), 8.00 (m, 1H), 7.72 (dt, 1H, J = 7.8, 1.4 Hz), 7.64 (t, 1H, J = 7.7 Hz), 7.53 (m, 1H), 7.26 (t, 2H, J = 8.3 Hz). ^{13}C NMR (DMSO-d_6, 100 MHz) δ 167.7, 158.7, 135.0, 132.2, 131.4, 131.1, 129.9, 129.5, 129.5, 112.8, 110.9. HRESIMS calculated for $C_{13}H_8F_2O_2$ (M − H) 233.0414, found 233.0410. Normal phase HPLC retention time: 12.1 min. Reverse phase HPLC retention time: 12.1 min. >97% pure.

2′,6′-Difluorobiphenyl-4-carboxylic Acid (20). ^{1}H NMR (DMSO-d_6, 400 MHz) δ 8.06 (AA'XX′, 2H, $J_{AA'} = J_{XX'}$ = 2.0 Hz, $J_{XA} = J_{X'A'}$ = 8.0 Hz, $J_{X'A} = J_{XA'}$ = 0.7 Hz, $\nu_A = \nu_{A'}$ = 3243.6 Hz, $\nu_X = \nu_{X'}$ = 3018.6 Hz), 7.60 (AA′XX', 2H, as above), 7.54 (m, 1H), 7.27 (t, 2H, J = 8.3 Hz). ^{13}C NMR (DMSO-d_6, 100 MHz) δ 171.0, 164.0, 134.1, 125.7, 122.0, 121.9, 121.1, 103.4. HRESIMS calculated for $C_{13}H_8F_2O_2$ (M − H) 233.0414, found 233.0425. Normal phase HPLC retention time: 14.5 min. Reverse phase HPLC retention time: 12.1 min. >99% pure.

Biphenyl-4-carboxylic Acid (22). ^{1}H NMR (DMSO-d_6, 400 MHz) δ 13.07 (br s, 1H), 8.03 (AA'XX′, 2H, $J_{AA'} = J_{XX'}$ = 1.8 Hz, $J_{XA} = J_{X'A'}$ = 8.3 Hz, $J_{X'A} = J_{XA'}$ = 0.3 Hz, $\nu_A = \nu_{A'}$ = 3210.7 Hz, $\nu_X = \nu_{X'}$ = 3122.0 Hz), 7.81 (AA′XX', 2H, as above), 7.75 (m, 2H), 7.51 (tt, 2H, J = 7.2, 1.1 Hz), 7.43 (tt, 1H, J = 7.4, 1.2 Hz). ^{13}C NMR (DMSO-d_6, 100 MHz) δ 167.2, 144.2, 139.0, 130.0, 129.8, 129.1, 128.3, 127.0, 126.8. HREIMS calculated for $C_{13}H_{10}O_2$ (M^+) 198.0683, found 198.0683. Normal phase HPLC retention time: 13.8 min. Reverse phase HPLC retention time: 12.2 min. >99% pure.

Methyl 5-Iodo-2-methoxybenzoate.[60] TMS-diazomethane (19.25 mL, 38.50 mmol, 2 M solution in hexane) was added to a solution of 5-iodosalicylic acid (5.08 g, 19.24 mmol) in MeOH (20 mL) and stirred at room temperature for 11 h. Upon completion, the reaction was concentrated in vacuo and the residue was carried onto the next step without further purification.

Methyl iodide (2.40 mL, 38.48 mmol) and K_2CO_3 (10.60 g, 76.96 mmol) were added to a solution of 5-iodo-2-methoxybenzoate (5.37 g, 19.24 mmol) in DMF (20 mL) and stirred at room temperature under Ar for 24 h. Upon completion, ethyl acetate was added and the reaction was washed with 1% HCl (2 × 20 mL), brine (1×), dried over $MgSO_4$, and concentrated in vacuo. The residue was purified by flash chromatography (3:1 hexane: ethyl acetate) to afford methyl 5-iodo-2-methoxybenzoate (4.93 g, 88%) as a white solid. ^{1}H NMR (DMSO-d_6, 400 MHz) δ 7.90 (d, 1H, J = 2.4 Hz), 7.80 (dd, 1H, J = 8.8, 2.4 Hz), 6.96 (d, 1H, J = 9.0 Hz), 3.81 (s, 3H), 3.79 (s, 3H). ^{13}C NMR (DMSO-d_6, 100 MHz) δ 164.7, 158.0, 141.6, 138.5, 122.2, 115.2, 82.1, 55.9, 52.0. HREIMS calculated for $C_9H_9IO_3$ (M^+) 291.9608, found 291.9596.

General Procedure for Pd-Mediated Suzuki Coupling Reactions To Prepare 23, 24, 25, 26, 27. To a solution of methyl 5-iodo-2-methoxybenzoate (1.0 equiv) dissolved in enough toluene to give a concentration of 0.08 M was added a solution of phenyl boronic acid (2.0 equiv) dissolved in EtOH to give a 0.8 M solution of boronic acid. A 2 M aqueous solution of Na_2CO_3 was added to give a final reaction concentration of 0.06 M with respect to the methoxybenzoate, followed by addition of $Pd(PPh_3)_4$ (10.0 mol %). The reaction was stirred at 60 °C under Ar for 15 h and, upon completion, was cooled to room temperature, extracted with CH_2Cl_2 (2×), washed with brine (1×), dried over $MgSO_4$, and concentrated in vacuo. The residue was purified by flash chromatography (3:1 hexane: ethyl acetate) to afford the methylated salicylates.

To a solution of the methylated salicylate (1.0 equiv) in enough CH_2Cl_2 to give a concentration of 0.06 M was added BBr_3 (2.0 equiv, 1 M solution in CH_2Cl_2). The reaction was

stirred at room temperature under Ar for 4 h and, upon completion, was quenched with H_2O (10 mL), extracted with CH_2Cl_2 (2×), washed with brine (1×), dried over $MgSO_4$, and concentrated in vacuo. The residue was carried onto the next step without further purification.

To a solution of methyl ester (1.0 equiv) in THF:MeOH:H_2O (1:1:1) at a concentration of 0.06 M was added LiOH·H_2O (3.0 equiv). The reaction was stirred at room temperature for 4 h and, upon completion, was acidified with 30% HCl, extracted with ethyl acetate (3 × 5 mL), dried over $MgSO_4$, and concentrated in vacuo. The residue was purified by flash chromatography (CH_2Cl_2, 1% MeOH, 0.2% acetic acid) to afford the biphenyl salicylates as white solids in 12−42% yields.

Characterization for 23, 24, 25, 26, and 27.

4′-Fluoro-4-hydroxybiphenyl-3-carboxylic Acid (23). ^{1}H NMR (CD_3OD, 400 MHz) δ 8.01 (d, 1H, J = 2.5 Hz), 7.65 (dd, 1H, J = 8.7, 2.5 Hz), 7.51 (m, 2H), 7.11 (tt, 2H, J = 10.0, 3.0 Hz), 6.97 (d, 1H, J = 8.7 Hz. ^{13}C NMR (CD_3OD, 100 MHz) δ 173.5, 165.0, 162.7, 137.7, 135.1, 132.6, 129.6, 129.3, 118.9, 116.7, 116.6, 114.2. HRESIMS calculated for $C_{13}H_9FO_3$ (M − H) 231.0459, found 231.0457. Normal phase HPLC retention time: 14.2 min. Reverse phase HPLC retention time: 12.8 min. >99% pure.

2′-Fluoro-4-hydroxybiphenyl-3-carboxylic Acid (24). ^{1}H NMR (CD_3OD, 400 MHz) δ 7.98 (dd, 1H, J = 2.2, 1.4 Hz), 7.59 (ddd, 1H, J = 8.7, 2.4, 1.7 Hz), 7.36 (td, 1H, J = 7.8, 1.7 Hz), 7.26 (dddd, 1H, J = 9.9, 7.4, 4.9, 1.7 Hz), 7.16 (td, 1H, J = 7.5, 1.2 Hz), 7.10 (ddd, 1H, J = 11.1, 8.2, 1.3 Hz), 6.95 (d, 1H, J = 8.5 Hz). ^{13}C NMR (CD_3OD, 100 MHz) δ 173.5, 162.9, 162.4, 137.2, 131.8, 130.2, 130.1, 129.1, 128.1, 125.8, 118.5, 117.1, 114.0. HRESIMS calculated for $C_{13}H_9FO_3$ (M − H) 231.0457, found 231.0446. Normal phase HPLC retention time: 13.8 min. Reverse phase HPLC retention time: 12.7 min. >99% pure.

3′,5′-Difluoro-4-hydroxybiphenyl-3-carboxylic Acid (25). ^{1}H NMR (CD_3OD, 400 MHz) δ 8.07 (d, 1H, J = 2.5 Hz), 7.73 (dd, 1H, J = 8.5, 2.7 Hz), 7.15 (m, 2H), 7.01 (d, 1H, J = 8.9 Hz), 6.86 (tt, 1H, J = 9.0, 2.5 Hz). ^{13}C NMR (CD_3OD, 100 MHz) δ 173.3, 166.3, 163.8, 145.1, 135.2, 131.0, 129.8, 119.2, 114.4, 110.4, 103.0. HRESIMS calculated for $C_{13}H_8F_2O_3$ (M − H) 249.0363, found 249.0356. Normal phase HPLC retention time: 14.5 min. Reverse phase HPLC retention time: 13.3 min. >99% pure.

2′,4′-Dichloro-4-hydroxybiphenyl-3-carboxylic Acid (26). ^{1}H NMR (CD_3OD, 400 MHz) δ 7.83 (d, 1H, J = 2.2 Hz), 7.70 (d, 1H, J = 2.0 Hz), 7.58 (dd, 1H, J = 8.6, 2.4 Hz), 7.48 (*A*BX, 1H, J_{AB} = 8.4 Hz, J_{AX} = 2.2 Hz, J_{BX} = 0.0 Hz, ν_A = 2989.4 Hz, ν_B = 2973.0 Hz), 7.44 (A*B*X, 1H, as above), 7.06 (d, 1H, J = 8.7 Hz). ^{13}C NMR (CD_3OD, 100 MHz) δ 171.6, 160.8, 137.5, 136.4, 132.8, 132.6, 132.4, 130.8, 129.2, 128.5, 127.7, 117.2, 112.9. HRESIMS calculated for $C_{13}H_8Cl_2O_3$ (M − H) 280.9772, found 280.9782. Normal phase HPLC retention time: 13.1 min. Reverse phase HPLC retention time: 14.4 min. >99% pure.

4-Hydroxybiphenyl-3-carboxylic Acid (27). ^{1}H NMR (CD_3OD, 400 MHz) δ 8.08 (d, 1H, J = 2.4 Hz), 7.73 (dd, 1H, J = 8.7, 2.3 Hz), 7.54 (m, 2H), 7.41 (tt, 2H, J = 7.3, 1.8 Hz), 7.29 (tt, 1H, J = 7.8, 1.7 Hz), 7.38 (dddd, 1H, J = 8.8, 6.4 Hz), 7.05 (d, 1H, J = 8.7 Hz), 6.93 (m, 1H), 6.90 (ddd, 1H, J = 7.3, 1.9 Hz), 7.00 (d, 1H, J = 8.5 Hz). ^{13}C NMR (CD_3OD, 100 MHz) δ 161.5, 140.1, 134.0, 132.4, 128.7, 128.3, 126.9, 126.3, 117.5, 112.9. HRESIMS calculated for $C_{13}H_{10}O_3$ (M − H) 213.0552, found 213.0545. Normal phase HPLC retention time: 12.9 min. Reverse phase HPLC retention time: 12.6 min. >99% pure.

4-Bromo-2,6-difluoroanisole.[61] Methyl iodide (580 μL, 10.06 mmol) and K_2CO_3 (2.80 g, 20.12 mmol) were added to a solution of 4-bromo-2,6-difluorophenol (1.05 g, 5.03 mmol) in DMF (10 mL) and stirred at room temperature under Ar for 24 h. Upon completion, ethyl acetate was added and the reaction was washed with 1% HCl (2 × 20 mL), brine (1×), dried over $MgSO_4$, and concentrated in vacuo. The residue was purified by flash chromatography (hexane) to afford 4-bromo-2,6-difluoroanisole (747 mg, 67%) as a white solid. ^{1}H NMR ($CDCl_3$, 400 MHz) δ 7.06 (m, 2H), 3.97 (q, 3H, J = 1.1 Hz). ^{13}C NMR ($CDCl_3$, 100 MHz) δ 155.8, 136.3, 116.2, 113.8, 61.9. LREIMS found for $C_7H_5F_2OBr$ (M^+) 223.0.

4-Bromo-2,6-dichloroanisole.[62] Methyl iodide (467 μL, 8.12 mmol) and K_2CO_3 (2.24 g, 16.24 mmol) were added to a solution of 4-bromo-2,6-dichlorophenol (982 mg, 4.06 mmol) in DMF (10 mL) and stirred at room temperature under Ar for 40 min. Upon completion, ethyl acetate was added and the reaction was washed with 1% HCl (2 × 20 mL), brine (1×), dried over $MgSO_4$, and concentrated in vacuo. The residue was purified by flash chromatography (hexane) to afford 4-bromo-2,6-dichloroanisole (768 mg, 74%) as a white solid. ^{1}H NMR (DMSO-d_6, 400 MHz) δ 7.75 (s, 2H), 3.81 (s, 3H). ^{13}C NMR (DMSO-d_6, 100 MHz) δ 151.3, 131.5, 129.6, 116.5, 60.6. HREIMS calculated for $C_7H_5BrCl_2O$ (M^+) 253.8905, found 253.8901.

General Procedure for Pd-Mediated Suzuki Coupling Reactions To Prepare 28, 29, 30, 31. To a solution of the appropriate halo-anisole (1.0 equiv) dissolved in enough toluene to give a concentration of 0.25 M was added a solution of phenyl boronic acid (2.0 equiv) dissolved in EtOH to give a 1.5 M solution of boronic acid. A 2 M aqueous solution of Na_2CO_3 was added to give a final reaction concentration of 0.08 M with respect to the halo-anisole, followed by addition of Pd(PPh_3)$_4$ (10.0 mol %). The reaction was stirred at 65 °C for 17 h and, upon completion, was cooled to room temperature, extracted with CH_2Cl_2 (2×), washed with brine (1×), dried over $MgSO_4$, and concentrated in vacuo. The residue was purified by flash chromatography (20:1 hexane:ethyl acetate) to afford the methylated biphenyl as a white solid.

To a solution of the methylated biphenyl (1.0 equiv) in enough CH_2Cl_2 to give a concentration of 0.20 M was added BBr_3 (2.0 equiv, 1 M solution in CH_2Cl_2). The reaction was stirred at room temperature under Ar for 3 h and, upon completion, was quenched with H_2O (10 mL), extracted with CH_2Cl_2 (2×), washed with brine (1×), dried over $MgSO_4$, and concentrated in vacuo. The residue was carried onto the next step without further purification.

To a solution of methyl ester (1.0 equiv) in THF:MeOH:H_2O (1:1:1) at a concentration of 0.04 M was added LiOH·H_2O (3.0 equiv). The reaction was stirred at room temperature for 5 h and, upon completion, was acidified with 30% HCl, extracted with ethyl acetate (3 × 5 mL), dried over $MgSO_4$, and concentrated in vacuo. The residue was purified by flash chromatography (CH_2Cl_2, 1% MeOH, 0.2% acetic acid) to afford the biphenyl products as white solids in 14−39% yields.

Characterization for 28, 29, 30, and 31.

3′,5′-Difluoro-4′-hydroxybiphenyl-3-carboxylic Acid (28). ^{1}H NMR (DMSO-d_6, 400 MHz) δ 10.60 (br s, 1H), 8.14 (t, 1H, J = 1.7 Hz), 7.91 (dt, 1H, J = 7.7, 1.1 Hz), 7.88 (ddd, 1H, J = 8.0, 2.0, 1.1 Hz), 7.55 (t, 1H, J = 7.9 Hz), 7.41 (m, 2H). ^{13}C NMR (DMSO-d_6, 100 MHz) δ 167.3, 154.0, 151.5, 138.4, 133.6, 131.6, 130.8, 129.9, 129.4, 128.4, 127.1, 110.3. HRESIMS calculated for $C_{13}H_8F_2O_3$ (M − H) 249.0363, found 249.0358. Normal phase HPLC retention time: 18.3 min. Reverse phase HPLC retention time: 10.5 min. >98% pure.

3′,5′-Difluoro-4′-hydroxybiphenyl-4-carboxylic Acid (29). ^{1}H NMR (DMSO-d_6, 400 MHz) δ 7.98 (*AA*′XX′, 2H, $J_{AA'}$ = $J_{XX'}$ = 1.7 Hz, J_{XA} = $J_{X'A'}$ = 8.2 Hz, $J_{X'A}$ = $J_{XA'}$ = 0.5 Hz, ν_A = $\nu_{A'}$ = 3189.9 Hz, ν_X = $\nu_{X'}$ = 3122.0 Hz), 7.81 (AA′*XX*′, 2H, as above), 7.51 (m, 2H). ^{13}C NMR (DMSO-d_6, 100 MHz) δ 167.7, 154.5, 142.5, 136.0, 130.5, 130.5, 130.4, 126.9, 111.0. HRESIMS calculated for $C_{13}H_8F_2O_3$ (M − H) 249.0363, found 249.0375. Normal phase HPLC retention time: 18.9 min. Reverse phase HPLC retention time: 10.2 min. >99% pure.

3′,5′-Dichloro-4′-hydroxybiphenyl-3-carboxylic Acid (30). ^{1}H NMR (DMSO-d_6, 400 MHz) δ 8.13 (t, 1H, J = 1.6 Hz), 7.91 (m, 2H), 7.70 (s, 2H), 7.56 (t, 1H, J = 7.8 Hz). ^{13}C NMR (DMSO-d_6, 100 MHz) δ 167.2, 149.0, 137.9, 132.2, 131.6, 130.8, 129.3, 128.4, 127.1, 126.8, 122.9, 123.0. HRESIMS calculated for $C_{13}H_8Cl_2O_3$ (M − H) 280.9772, found 280.9767. Normal phase HPLC retention time: 16.2 min. Reverse phase HPLC retention time: 11.6 min. >99% pure.

3′,5′-Dichloro-4′-hydroxybiphenyl-4-carboxylic Acid (31). ^{1}H NMR (DMSO-d_6, 400 MHz) δ 7.98 (*AA′*XX′, 2H, $J_{AA'} = J_{XX'} = 1.7$ Hz, $J_{XA} = J_{X'A'} = 8.1$ Hz, $J_{X'A} = J_{XA'} = 0.5$ Hz, $\nu_A = \nu_{A'} = 3189.9$ Hz, $\nu_X = \nu_{X'} = 3110.0$ Hz), 7.81 (AA′*XX*′, 2H, as above), 7.78 (s, 2H). ^{13}C NMR (DMSO-d_6, 100 MHz) δ 167.2, 141.8, 141.7, 134.7, 129.9, 129.7, 126.9, 126.4, 123.0. HRESIMS calculated for $C_{13}H_8Cl_2O_3$ (M − H) 280.9772, found 280.9785. Normal phase HPLC retention time: 15.9 min. Reverse phase HPLC retention time: 11.4 min. >97% pure.

Methyl-2′,4′-difluoro-4-hydroxybiphenyl-3-carboxylate (32). TMS-diazomethane (5.87 mL, 11.75 mmol, 2M solution in hexane) was added to a solution of diflunisal (1.03 g, 4.11 mmol) in MeOH (10 mL) and stirred at room temperature for 5 h. Upon completion, the reaction was concentrated in vacuo and the residue was purified by flash chromatography (10:1 hexane:ethyl acetate) to afford **32** (774 mg, 71%) as a white solid. ^{1}H NMR ($CDCl_3$, 400 MHz) δ 7.97 (dd, 1H, J = 2.2, 1.3 Hz), 7.59 (dt, 1H, J = 8.8, 2.1 Hz), 7.36 (dq, 1H, J = 7.7, 1.5 Hz), 7.48 (td, 1H, J = 7.8, 1.7 Hz), 7.38 (dddd, 1H, J = 8.8, 6.4 Hz), 7.05 (d, 1H, J = 8.7 Hz), 6.93 (m, 1H), 6.90 (ddd, 1H, J = 10.6, 8.9, 2.5 Hz), 3.96 (s, 3H). ^{13}C NMR ($CDCl_3$, 100 MHz) δ 170.6, 163.6, 161.3, 158.5, 136.4, 131.2, 130.3, 126.2, 124.2, 118.0, 112.6, 111.8, 104.6, 52.6, 124.2. HRFABMS calculated for $C_{14}H_{10}F_2O_3$ (M^+) 264.0596, found 264.0598. Normal phase HPLC retention time: 6.9 min. Reverse phase HPLC retention time: 14.7 min. >99% pure.

2′,4′-Difluoro-4-methoxybiphenyl-3-carboxylic Acid (33). Methyl iodide (350 μL, 1.16 mmol) and K_2CO_3 (320 mg, 2.32 mmol) were added to a solution of **32** (152 mg, 0.58 mmol) in DMF (4 mL) and stirred at room temperature under Ar for 14 h. Upon completion, ethyl acetate was added and the reaction was washed with 1% HCl (2 × 20 mL), brine (1×), dried over $MgSO_4$, and concentrated in vacuo and carried onto the next step without further purification.

$LiOH·H_2O$ (60 mg, 1.43 mmol) was added to a solution of fully methylated diflunisal (140 mg, 0.50 mmol) in MeOH:THF:H_2O (4.5 mL 1:1:1), and stirred at room temperature for 4 h. Upon completion, the reaction was acidified with 30% HCl, extracted with ethyl acetate (3 × 5 mL), dried over $MgSO_4$, and concentrated in vacuo. The residue was purified by flash chromatography (2:1 ethyl acetate:hexane, 1% acetic acid) to afford **33** (122 mg, 93%) as a white solid. ^{1}H NMR ($CDCl_3$, 400 MHz) δ 10.77 (br s, 1H), 8.31 (dd, 1H, J = 2.5, 0.9 Hz), 7.75 (dt, 1H, J = 8.6, 2.1 Hz), 7.41 (dt, 1H, J = 8.9, 6.6 Hz), 7.15 (d, 1H, J = 8.8 Hz), 6.94 (m, 1H), 4.13 (s, 3H). ^{13}C NMR ($CDCl_3$, 100 MHz) δ 177.7, 161.4, 158.2, 135.7, 133.9, 131.4, 129.0, 123.5, 118.1, 112.2, 112.0, 104.6, 56.9. HRESIMS calculated for $C_{14}H_{10}F_2O_3$ (M − H) 263.0520, found 263.0514. Normal phase HPLC retention time: 21.6 min. Reverse phase HPLC retention time: 11.9 min. >99% pure.

General Procedure for Pd-Mediated Suzuki Coupling Reactions To Prepare 39, 40, 41. To a solution of aryl iodide (1.0 equiv) in enough toluene to give a concentration of 0.07 M was added an appropriate formyl phenylboronic acid dissolved in enough EtOH to provide a concentration of 0.4 M boronic acid. A 2 M aqueous solution of Na_2CO_3 was added to give a final reaction concentration of 0.04 M with respect to aryl iodide, followed by addition of $Pd(PPh_3)_4$ (3.0 mol %). The reaction was heated to reflux under Ar for 18 h and, upon completion, was cooled to room temperature, extracted with CH_2Cl_2 (2×), washed with brine (1×), dried over $MgSO_4$, and concentrated in vacuo. The residue was purified by flash chromatography (40:1 hexane:ethyl acetate) to afford the biphenyl aldehydes as white solids in 40−91% yields.

Characterization for 39, 40, 41.

3′,5′-Dichloro-3-formylbiphenyl (39). ^{1}H NMR ($CDCl_3$, 400 MHz) δ 10.09 (s, 1H), 8.04 (t, 1H, J = 1.8 Hz), 7.91 (dt, 1H, J = 7.6, 1.3 Hz), 7.80 (ddd, 1H, J = 7.8, 2.0, 1.3 Hz), 7.64 (t, 1H, J = 7.8 Hz), 7.49 (d, 2H, J = 1.8 Hz), 7.38 (t, 1H, J = 1.9 Hz). ^{13}C NMR ($CDCl_3$, 100 MHz) δ 192.0, 142.8, 139.7, 137.2, 135.8, 133.0, 130.1, 130.0, 128.1, 128.0, 125.9. HR-FABMS calculated for $C_{13}H_8Cl_2O$ (M + H) 251.0027, found 251.0027. Normal phase HPLC retention time: 8.0 min. Reverse phase HPLC retention time: 15.2 min. >99% pure.

3′,5′-Dichloro-4-formylbiphenyl (40). ^{1}H NMR ($CDCl_3$, 400 MHz) δ 7.99 (*AA′*XX′, 2H, $J_{AA'} = J_{XX'} = 2.1$ Hz, $J_{XA} = J_{X'A'} = 8.5$ Hz, $J_{X'A} = J_{XA'} = 0.7$ Hz, $\nu_A = \nu_{A'} = 3193.7$ Hz, $\nu_X = \nu_{X'} = 3077.8$ Hz), 7.70 (AA′*XX*′, 2H, as above), 7.47 (t, 1H, J = 1.9 Hz), 7.39 (d, 2H, J = 1.9 Hz). ^{13}C NMR ($CDCl_3$, 100 MHz) δ 191.8, 144.4, 142.9, 136.2, 135.8, 130.6, 128.5, 127.9, 126.1. HREIMS calculated for $C_{13}H_8Cl_2O$ (M − H) 248.9873, found 248.9874. Normal phase HPLC retention time: 7.9 min. Reverse phase HPLC retention time: 15.2 min. >99% pure.

3′,5′-Dichloro-2-formylbiphenyl (41). ^{1}H NMR ($CDCl_3$, 400 MHz) δ 9.98 (s, 1H), 8.03 (dd, 1H, J = 7.8, 1.3 Hz), 7.66 (td, 1H, J = 7.6, 1.5 Hz), 7.55 (tt, 1H, J = 7.6, 1.0 Hz), 7.44 (t, 1H, J = 1.9 Hz), 7.39 (dd, 1H, J = 7.7, 1.0 Hz), 7.27 (d, 2H, J = 1.9 Hz). ^{13}C NMR ($CDCl_3$, 100 MHz) δ 191.4, 142.9, 141.0, 135.3, 134.0, 133.7, 130.7, 129.0, 128.5, 128.4, 128.4. HR-FABMS calculated for $C_{13}H_8Cl_2O$ (M + H) 251.0030, found 251.0029. Normal phase HPLC retention time: 7.0 min. Reverse phase HPLC retention time: 14.9 min. >99% pure.

General Procedure for $KMnO_4$ Oxidation Reactions To Prepare 45, 46, 47. To a solution of biphenyl aldehyde (1.0 equiv) in enough acetone to give a concentration of 0.07 M was added $KMnO_4$ (2.0 equiv) in enough H_2O to give a concentration of 0.2 M permanganate. The reaction was stirred for 16 h at room temperature and, upon completion, was concentrated in vacuo, and the resulting residue was redissolved in 10:1 CH_2Cl_2:MeOH and filtered through a plug of glass wool. The crude product was purified by flash chromatography (10:1 CH_2Cl_2:MeOH) to afford the carboxylic acids as white solids in 82−100% yields.

Characterization for 45, 46, 47.

2′,4′-Dichlorobiphenyl-3-carboxylic Acid (45). ^{1}H NMR (DMSO-d_6, 400 MHz) δ 8.22 (br s, 1H), 8.00 (br s, 1H), 7.94 (d, 1H, J = 7.5 Hz), 7.76 (s, 2H), 7.63 (s, 1H), 7.60 (br s, 1H). ^{13}C NMR (DMSO-d_6, 100 MHz) δ 168.0, 143.7, 138.1, 135.4, 131.6, 129.9, 127.9, 126.2. HRESIMS calculated for $C_{13}H_8Cl_2O_2$ (M − H) 264.9823, found 264.9810. Normal phase HPLC retention time: 12.3 min. Reverse phase HPLC retention time: 14.2 min. >99% pure.

2′,4′-Dichlorobiphenyl-4-carboxylic Acid (46). ^{1}H NMR (CD_3OD, 400 MHz) δ 8.11 (br s, 2H) 7.72 (m, 2H), 7.64 (d, 2H, J = 1.9 Hz), 7.46 (t, 1H, J = 1.7 Hz). ^{13}C NMR (DMSO-d_6, 100 MHz) δ 170.3, 140.6, 135.2, 127.2, 126.4, 119.3, 118.6, 117.4. HRESIMS calculated for $C_{13}H_8Cl_2O_2$ (M − H) 264.9830, found 264.9823. Normal phase HPLC retention time: 12.5 min. Reverse phase HPLC retention time: 14.4 min. >99% pure.

2′,4′-Dichlorobiphenyl-2-carboxylic Acid (47). ^{1}H NMR (DMSO-d_6, 400 MHz) δ 7.75 (br s, 1H), 7.56 (s, 2H), 7.48 (m, 2H), 7.36 (m, 2H). ^{13}C NMR (DMSO-d_6, 100 MHz) δ 170.1, 152.5, 145.2, 133.3, 130.0, 129.6, 128.0, 127.2, 126.3. HRESIMS calculated for $C_{13}H_8Cl_2O_2$ (M − H) 264.9823, found 264.9834. Normal phase HPLC retention time: 11.4 min. Reverse phase HPLC retention time: 13.6 min. >99% pure.

General Procedure for $NaBH_4$ Reduction Reactions To Prepare 48, 49, 50. To a solution of biphenyl aldehyde (1.0 equiv) in enough MeOH to give a concentration of 0.1 M was added $NaBH_4$ (2.0 equiv) in enough MeOH to give a concentration of 0.3 M borohydride. The reaction was stirred at 0 °C, slowly warmed to room temperature, and after stirring for 16 h, was concentrated in vacuo and purified by flash chromatography (3:1 hexane:ethyl acetate) to afford the biphenyl alcohols as white solids in 94−100% yields.

Characterization for 48, 49, 50.

3′,5′-Dichlorobiphenyl-3-yl-methanol (48). ^{1}H NMR ($CDCl_3$, 400 MHz) δ 7.54 (m, 1H), 7.46 (d, 2H, J = 1.8 Hz), 7.45 (m, 2H), 7.39 (m, 1H), 7.34 (t, 1H, J = 1.9 Hz), 4.77 (s, 2H), 1.90 (br s, 1H). ^{13}C NMR ($CDCl_3$, 100 MHz) δ 144.1, 141.9, 139.0, 135.5, 129.5, 127.4, 127.1, 126.5, 125.8, 125.7, 65.3. HREIMS calculated for $C_{13}H_{10}Cl_2O$ (M^+) 252.0103, found 252.0109. Normal phase HPLC retention time: 13.9 min. Reverse phase HPLC retention time: 14.0 min. >99% pure.

3′,5′-Dichlorobiphenyl-4-yl-methanol (49). ^{1}H NMR ($CDCl_3$, 400 MHz) δ 7.53 (*AA′*XX′, 2H, $J_{AA'} = 1.9$ Hz, $J_{XX'} = 3.1$ Hz, $J_{XA} = 8.7$ Hz, $J_{X'A'} = 6.4$ Hz, $J_{X'A} = J_{XA'} = 0.5$ Hz, $\nu_A = \nu_{A'} = 3009.8$ Hz, $\nu_X = \nu_{X'} = 2977.8$ Hz), 7.45 (AA′*XX*′, 2H, as

above), 7.45 (d, 2H, $J = 1.9$ Hz), 7.33 (t, 1H, $J = 1.9$ Hz), 4.75 (br d, 2H, $J = 4.8$ Hz), 1.81 (br t, 1H, $J = 5.2$ Hz). ^{13}C NMR ($CDCl_3$, 100 MHz) δ 144.0, 141.4, 138.0, 135.5, 127.8, 127.4, 127.4, 125.8, 65.1. HREIMS calculated for $C_{13}H_{10}Cl_2O$ (M^+) 251.0110, found 252.0109. Normal phase HPLC retention time: 15.4 min. Reverse phase HPLC retention time: 14.0 min >97% pure.

3′,5′-Dichlorobiphenyl-2-yl-methanol (50). ^{1}H NMR ($CDCl_3$, 400 MHz) δ 7.55 (dd, 1H, $J = 7.5$, 1.3 Hz), 7.43 (td, 2H, $J = 7.5$, 1.4 Hz), 7.38 (m, 2H), 7.29 (d, 2H, $J = 1.9$ Hz), 7.24 (dd, 1H, $J = 7.4$, 1.4 Hz), 4.58 (s, 2H), 1.79 (s, 1H). ^{13}C NMR ($CDCl_3$, 100 MHz) δ 143.7, 138.9, 137.9, 134.9, 130.0, 129.0, 128.9, 128.2, 127.9, 127.6, 63.0. HREIMS calculated for $C_{13}H_{10}Cl_2O$ (M^+) 252.0110, found 252.0109. Normal phase HPLC retention time: 11.5 min. Reverse phase HPLC retention time: 14.0 min >99% pure.

General Procedure for Pd-Mediated Suzuki Coupling Reactions To Prepare 54 and 55. To a solution of the appropriate iodobenzaldehyde (1.0 equiv) in enough toluene to give a concentration of 0.07 M was added 3,5-difluorophenyl boronic acid (2.0 equiv) dissolved in enough EtOH to provide a concentration of 1.0 M boronic acid. A 2 M aqueous solution of Na_2CO_3 was added to give a final reaction concentration of 0.04 M with respect to iodobenzaldehyde, followed by addition of $Pd(PPh_3)_4$ (4.0 mol %). The reaction was stirred at 60 °C for 17 h and, upon completion, was cooled to room temperature, extracted with CH_2Cl_2 (2×), washed with brine (1×), dried over $MgSO_4$, and concentrated in vacuo. The residue was purified by flash chromatography (10:1 hexane:ethyl acetate) to afford the biphenyl aldehydes as white solids in 78−80% yields.

Characterization for 54 and 55.

3′,5′-Difluoro-3-formylbiphenyl (54). ^{1}H NMR ($CDCl_3$, 400 MHz) δ 10.06 (s, 1H), 8.02 (t, 1H, $J = 1.4$ Hz), 7.88 (dt, 1H, $J = 7.8$, 1.4 Hz), 7.78 (ddd, 2H, $J = 7.8$, 2.0, 1.2 Hz), 7.61 (t, 2H, $J = 7.7$), 7.10 (m, 2H), 6.80 (tt, 1H, $J = 8.8$, 2.3 Hz. ^{13}C NMR ($CDCl_3$, 100 MHz) δ 192.0, 164.8, 162.3, 143.0, 139.8, 137.1, 132.9, 129.9, 127.9, 110.4, 103.5. HRFABMS calculated for $C_{13}H_8F_2O$ (M + H) 219.0620, found 219.0621. Normal phase HPLC retention time: 8.9 min. Reverse phase HPLC retention time: 13.7 min >99% pure.

3′,5′-Difluoro-4-formylbiphenyl (55). ^{1}H NMR ($CDCl_3$, 400 MHz) δ 9.98 (s, 1H), 8.02 (dd, 1H, $J = 7.8$, 1.5 Hz), 7.65 (td, 1H, $J = 7.3$, 1.4 Hz), 7.54 (t, 1H, $J = 7.8$ Hz), 7.40 (dd, 1H, $J = 7.6$, 1.2 Hz), 6.90 (m, 3H). ^{13}C NMR ($CDCl_3$, 100 MHz) δ 191.5, 164.1, 161.6, 143.4, 141.3, 134.0, 133.7, 130.6, 129.0, 128.3, 113.3, 103.8. HRFABMS calculated for $C_{13}H_8F_2O$ (M + H) 219.0620, found 219.0621. Normal phase HPLC retention time: 7.0 min. Reverse phase HPLC retention time: 13.4 min >99% pure.

Acknowledgment. We thank R. Luke Wiseman and Ted Foss for technical assistance. This work was supported by The Skaggs Institute for Chemical Biology and the Lita Annenberg Hazen Foundation.

Supporting Information Available: Normal and reverse phase HPLC traces for compounds **2**, **3**, **8**, **9**, **11**, **12**, **15**−**20**, **22**−**33**, **39**−**41**, **45**−**50**, **54**, and **55**. This material is available free of charge via the Internet at http://pubs.acs.org.

References

(1) Colon, W.; Kelly, J. W. Partial Denaturation of Transthyretin is Sufficient for Amyloid Fibril Formation in Vitro. *Biochemistry* **1992**, *31*, 8654−60.
(2) Kelly, J. W. Alternative Conformations of Amyloidogenic Proteins Govern Their Behavior. *Curr. Opin. Struct. Biol.* **1996**, *6*, 11−7.
(3) Liu, K.; Cho, H. S.; Lashuel, H. A.; Kelly, J. W.; Wemmer, D. E. A Glimpse of a Possible Amyloidogenic Intermediate of Transthyretin. *Nat. Struct. Biol.* **2000**, *7*, 754−7.
(4) Westermark, P.; Sletten, K.; Johansson, B.; Cornwell, G. G., III. Fibril in Senile Systemic Amyloidosis is Derived from Normal Transthyretin. *Proc. Natl. Acad. Sci. U.S.A.* **1990**, *87*, 2843−5.
(5) Saraiva, M. J.; Costa, P. P.; Goodman, D. S. Biochemical Marker in Familial Amyloidotic Polyneuropathy, Portuguese Type. Family Studies on the Transthyretin (Prealbumin)-Methionine-30 Variant. *J. Clin. Invest.* **1985**, *76*, 2171−7.
(6) Jacobson, D. R.; Pastore, R. D.; Yaghoubian, R.; Kane, I.; Gallo, G.; Buck, F. S.; Buxbaum, J. N. Variant-Sequence Transthyretin (Isoleucine 122) in Late-Onset Cardiac Amyloidosis in Black Americans *N. Engl. J. Med.* **1997**, *336*, 466−73.
(7) Buxbaum, J. N.; Tagoe, C. E. The Genetics of the Amyloidoses. *Annu. Rev. Med.* **2000**, *51*, 543−569.
(8) Saraiva, M. J. Transthyretin mutations in health and disease. *Hum. Mutat.* **1995**, *5*, 191−6.
(9) Blake, C. C.; Geisow, M. J.; Oatley, S. J.; Rerat, B.; Rerat, C. Structure of Prealbumin: Secondary, Tertiary and Quaternary Interactions Determined by Fourier Refinement at 1.8 Å. *J. Mol. Biol.* **1978**, *121*, 339−56.
(10) Wojtczak, A.; Cody, V.; Luft, J. R.; Pangborn, W. Structures of Human Transthyretin Complexed with Thyroxine at 2.0 Angstrom Resolution and 3′,5′-Dinitro-*N*-acetyl-L-thyronine at 2.2 Angstrom Resolution. *Acta Crystallogr., Sect. D* **1996**, 758−810.
(11) Monaco, H. L.; Rizzi, M.; Coda, A. Structure of a Complex of Two Plasma Proteins: Transthyretin and Retinol-Binding Protein. *Science* **1995**, *268*, 1039−41.
(12) Lai, Z.; Colon, W.; Kelly, J. W. The Acid-Mediated Denaturation Pathway of Transthyretin Yields a Conformational Intermediate that can Self-Assemble into Amyloid. *Biochemistry* **1996**, *35*, 6470−82.
(13) Holmgren, G.; Ericzon, B. G.; Groth, C. G.; Steen, L.; Suhr, O.; Andersen, O.; Wallin, B. G.; Seymour, A.; Richardson, S.; Hawkins, P. N.; Pepys, M. B. Clinical Improvement and Amyloid Regression After Liver Transplantation in Hereditary Transthyretin Amyloidosis. *Lancet* **1993**, *341*, 1113−6.
(14) Suhr, O. B.; Ericzon, B. G.; Friman, S. Long-Term Follow-Up of Survival of Liver Transplant Recipients with Familial Amyloid Polyneuropathy (Portuguese Type). *Liver Transpl.* **2002**, *8*, 787−94.
(15) Dubrey, S. W.; Davidoff, R.; Skinner, M.; Bergethon, P.; Lewis, D.; Falk, R. H. Progression of Ventricular Wall Thickening After Liver Transplantation for Familial Amyloidosis. *Transplantation* **1997**, *64*, 74−80.
(16) Yazaki, M.; Tokuda, T.; Nakamura, A.; Higashikata, T.; Koyama, J.; Higuchi, K.; Harihara, Y.; Baba, S.; Kametani, F.; Ikeda, S. Cardiac Amyloid in Patients with Familial Amyloid Polyneuropathy Consists of Abundant Wild-Type Transthyretin. *Biochem. Biophys. Res. Commun.* **2000**, *274*, 702−6.
(17) Cornwell, C. G., III; Murdoch, W. L.; Kyle, R. A.; Westermark, P.; Pitkanen, P. Frequency and Distribution of Senile Cardiovascular Amyloid. A Clinicopathologic Correlation. *Am. J. Med.* **1983**, *75*, 618−623.
(18) Miroy, G. J.; Lai, Z.; Lashuel, H. A.; Peterson, S. A.; Strang, C.; Kelly, J. W. Inhibiting Transthyretin Amyloid Fibril Formation Via Protein Stabilization. *Proc. Natl. Acad. Sci. U.S.A.* **1996**, *93*, 15051−6.
(19) Klabunde, T.; Petrassi, H. M.; Oza, V. B.; Raman, P.; Kelly, J. W.; Sacchettini, J. C. Rational Design of Potent Human Transthyretin Amyloid Disease Inhibitors. *Nat. Struct. Biol.* **2000**, *7*, 312−21.
(20) Baures, P. W.; Peterson, S. A.; Kelly, J. W. Discovering Transthyretin Amyloid Fibril Inhibitors by Limited Screening. *Bioorg. Med. Chem.* **1998**, *6*, 1389−401.
(21) Petrassi, H. M.; Klabunde, T.; Sacchettini, J.; Kelly, J. W. Structure-Based Design of *N*-Phenyl Phenoxazine Transthyretin Amyloid Fibril Inhibitors. *J. Am. Chem. Soc.* **2000**, *122*, 2178−2192.
(22) Baures, P. W.; Oza, V. B.; Peterson, S. A.; Kelly, J. W. Synthesis and Evaluation of Inhibitors of Transthyretin Amyloid Formation Based on the Non-Steroidal Antiinflammatory Drug, Flufenamic Acid. *Bioorg. Med. Chem.* **1999**, *7*, 1339−47.
(23) Sacchettini, J. C.; Kelly, J. W. Therapeutic Strategies for Human Amyloid Diseases. *Nat. Rev. Drug Discuss.* **2002**, *1*, 267−275.
(24) Oza, V. B.; Smith, C.; Raman, P.; Koepf, E. K.; Lashuel, H. A.; Petrassi, H. M.; Chiang, K. P.; Powers, E. T.; Sacchettini, J.; Kelly, J. W. Synthesis, Structure, and Activity of Diclofenac Analogues as Transthyretin Amyloid Fibril Formation Inhibitors. *J. Med. Chem.* **2002**, *45*, 321−32.
(25) Hammarstrom, P.; Wiseman, R. L.; Powers, E. T.; Kelly, J. W. Preventing a Human Disease by Changing the Energetics of Protein Misfolding. *Science* **2003**, *299*, 713−716.
(26) Bartalena, L.; Robbins, J. Thyroid Hormone Transport Proteins. *Clin. Lab. Med.* **1993**, *13*, 583−98.
(27) Aldred, A. R.; Brack, C. M.; Schreiber, G. The Cerebral Expression of Plasma Protein Genes in Different Species. *Comp. Biochem. Physiol. B Biochem. Mol. Biol.* **1995**, *111*, 1−15.
(28) Mao, H. Y.; Hajduk, P. J.; Craig, R.; Bell, R.; Borre, T.; Fesik, S. W. Rational Design of Diflunisal Analogues with Reduced Affinity for Human Serum Albumin. *J. Am. Chem. Soc.* **2001**, *123*, 10429−10435.
(29) Blake, C. C.; Oatley, S. J. Protein-DNA and Protein-Hormone Interactions in Prealbumin: a Model of the Thyroid Hormone Nuclear Receptor? *Nature* **1977**, *268*, 115−20.

(30) Verbeeck, R. K.; Boel, A.; Buntinz, A.; De Schepper, P. J. Plasma Protein Binding and Interaction Studies with Diflunisal, A New Salicylate Analgesic. *Biochem. Pharm.* **1980**, *29*, 571−576.
(31) Nuernberg, B.; Koehler, G.; Brune, K. Pharmacokinetics of Diflunisal in Patients. *Clin. Pharmacokin.* **1991**, *20*, 81−89.
(32) Miyaura, N.; Yanagi, T.; Suzuki, A. The Palladium-Catalyzed Cross-Coupling Reaction of Phenylboronic Acid With Haloarenes in the Presence of Bases. *Synth. Commun.* **1981**, *11*, 513−519.
(33) Sharp, M. J.; Snieckus, V. Synthetic Connections to the Aromatic Directed Metalation Reaction−Unsymmetrical Biaryls By Palladium-Catalyzed Cross Coupling of Directed Metalation-Derived Arylboronic Acids With Aryl Halides. *Tetrahedron Lett.* **1985**, *26*, 5997−6000.
(34) Sharp, M. J.; Cheng, W.; Snieckus, V. Synthetic Connections to the Aromatic Directed Metalation Reaction−Functionalized Aryl Boronic Acids By Ipso Borodesilylation−General Syntheses of Unsymmetrical Biphenyls and Meta-Terphenyls. *Tetrahedron Lett.* **1987**, *28*, 5093−5096.
(35) Pozsgay, V.; Nanasi, P.; Neszmelyi, A. Synthesis, and Carbon-13 NMR Study, of *O*-α-L-Rhamnopyranosyl-(1 → 3)-*O*-α-L-Rhamnopyranosyl-(1 → 2)-L-Rhamnopyranose and *O*-α-L-Rhamnopyranosyl-(1 →3)-*O*-α-L-Rhamnopyransoyl-(1 → 3)-L-Rhamnopyranose, Constituents of Bacterial, Cell-Wall Polysaccharides. *Carbohydr. Res.* **1981**, *90*, 215−231.
(36) Guiles, J. W.; Johnson, S. G.; Murray, W. V. Solid-Phase Suzuki Coupling for C−C Bond Formation *J. Org. Chem.* **1996**, *61*, 5169−5171.
(37) Nicolaou, K. C.; Boddy, C. N. C.; Li, H.; Koumbis, A. E.; Hughes, R.; Natarajan, S.; Jain, N. F.; Ramanjulu, J. M.; Brase, S.; Solomon, M. E. Total Synthesis of Vancomycin−Part 2: Retrosynthetic Analysis, Synthesis of Amino Acid Building Blocks and Strategy Evaluations. *Chem. Eur. J.* **1999**, *5*, 2602−2621.
(38) Chu-Moyer, M. Y.; Ballinger, W. E.; Beebe, D. A.; Berger, R.; Coutcher, J. B.; Day, W. W.; Li, J. C.; Mylari, B. L.; Oates, P. J.; Weekly, R. M. Orally-Effective, Long-Acting Sorbitol Dehydrogenase Inhibitors: Synthesis, Structure−Activity Relationships, and In Vivo Evaluations of Novel Heterocycle-Substituted Piperazino-Pyrimidines. *J. Med. Chem.* **2002**, *45*, 511−528.
(39) Song, X. P.; He, H. T.; Siahaan, T. J. Synthesis of Cyclic Prodrugs of Aggrastat and its Analogue with a Modified Phenylpropionic Acid Linker. *Org. Lett.* **2002**, *4*, 549−552.
(40) Nicolaou, K. C.; Namoto, K.; Ritzen, A.; Ulven, T.; Shoji, M.; Li, J.; D′Amico, G.; Liotta, D.; French, C. T.; Wartmann, M.; Altmann, K. H.; Giannakakou, P. Chemical Synthesis and Biological Evaluation of Cis- and Trans- 12,13-Cyclopropyl and 12,13-Cyclobutyl Epothilones and Related Pyridine Side Chain Analogues. *J. Am. Chem. Soc.* **2001**, *123*, 9313−9323.
(41) Purkey, H. E.; Dorrell, M. I.; Kelly, J. W. Evaluating the Binding Selectivity of Transthyretin Amyloid Fibril Inhibitors in Blood Plasma. *Proc. Natl. Acad. Sci. U.S.A.* **2001**, *98*, 5566−71.
(42) Steelman, S. L.; Cirillo, V. J.; Tempero, K. F. The Chemistry, Pharmacology and Clinical Pharmacology of Diflunisal. *Current Med. Res. Opin.* **1978**, *5*, 506−514.
(43) Hammarstrom, P.; Jiang, X.; Hurshman, A. R.; Powers, E. T.; Kelly, J. W. Sequence-Dependent Denaturation Energetics: A Major Determinant in Amyloid Disease Diversity. *Proc. Natl. Acad. Sci. U.S.A.* **2002**, *25*, 16427−32.
(44) Purkey, H. E.; Kent, K. C.; Smith, C.; Sacchettini, J. C.; Kelly, J. W. Unpublished Results.
(45) Hammarstrom, P.; Jiang, X.; Deechongkit, S.; Kelly, J. W. Anion Shielding of Electrostatic Repulsions in Transthyretin Modulates Stability and Amyloidosis: Insight into the Chaotrope Unfolding Dichotomy. *Biochemistry* **2001**, *40*, 11453−11459.
(46) Ma, J.; Lindquist, S. Conversion of PrP to a Self-Perpetuating PrPSc−Like Conformation in the Cytosol. *Science* **2002**, *298*, 1785−1788.
(47) Walsh, D. M. K. I.; Fadeeva, J. V.; Cullen, W. K.; Anwyl, R.; Wolfe, M. S.; Rowan, M. J.; Selkoe, D. J. Naturally Secreted Oligomers of Amyloid β Protein Potently Inhibit Hippocampal Long-Term Potentiation In Vivo. *Nature* **2002**, *416*, 535−539.
(48) Bucciantini, M. G. E.; Chiti, F.; Baroni, F.; Formigli, L.; Zurdo, J.; Taddei, N.; Ramponi, G.; Dobson, C. M.; Stefani, M. Inherent Toxicity of Aggregates Implies a Common Mechanism for Protein Mmisfolding Diseases. *Nature* **2002**, *416*, 507−511.
(49) Lashuel, H. A.; Hartley, D.; Petre, B. M.; Walz, T.; Lannsbury, P. T. Neurodegenerative Disease: Amyloid Pores from Pathogenic Mutations. *Nature* **2002**, *418*, 291.
(50) Klein, W. L.; Krafft, G. A.; Finch, C. E. Targeting Small Aβ Oligomers: The Solution to an Alzheimer's Disease Conundrum? *Trends Neurosci.* **2001**, *24*, 219−224.
(51) Otwinowski, Z.; Minor, W. Macromolecular Crystallography, Part A. In *Methods in Enzymology*; Carter, C. W., Sweet, R. M., Eds.; Academic Press: New York, 1997; Vol. 276, pp 307−326.
(52) Kissinger, C. R.; Gehlhaar, D. K.; Fogel, D. B. Rapid Automated Molecular Replacement by Evolutionary Search. *Acta Crystallogr., Sect. D* **1999**, *55*, 484−491.
(53) Brunger, A. T.; Adams, P. D.; Clore, G. M.; DeLano, W. L.; Gros, P.; Grosse-Kunstleve, R. W.; Jiang, J.-S.; Kuszewski, J.; Nilges, N.; Pannu, N. S.; Read, R. J.; Rice, L. M.; Simonson, T.; Warren, G. L. Crystallography & NMR System: A New Software Suite for Macromolecular Structure Determination. *Acta Crystallogr., Sect. D* **1998**, *54*, 905−921.
(54) Kantardjieff, K.; Höechtl, P.; Segelke, B.; Tao, F.-M.; Rupp, B. Concanavalin A in a dimeric crystal form: revisiting structural accuracy and molecular flexibility. *Acta Crystallogr., Sect. D* **2002**, *58*, 735−743.
(55) Bailey, S. The CCP4 Suite: Programs for Protein Crystallography. *Acta Crystallogr., Sect. D* **1994**, *50*, 760−763.
(56) Murshudov, G. N.; Vagin, A. A.; Dodson, E. J. Refinement of Macromolecular Structures by the Maximum-Likelihood Methodol. *Acta Crystallogr., Sect. D* **1997**, *53*, 240−255.
(57) Lashuel, H. A.; Lai, Z.; Kelly, J. W. Characterization of the Transthyretin Acid Denaturation Pathways by Analytical Ultracentrifugation: Implications for Wild-Type, V30M, and L55P Amyloid Fibril Formation. *Biochemistry* **1998**, *37*, 17851−64.
(58) Lashuel, H. A.; Wurth, C.; Woo, L.; Kelly, J. W. The Most Pathogenic Transthyretin Variant, L55P, Forms Amyloid Fibrils Under Acidic Conditions and Protofilaments Under Physiological Conditions. *Biochemistry* **1999**, *38*, 13560−73.
(59) Johansson, G.; Sundquist, S.; Nordvall, G.; Nilsson, B. M.; Brisander, M.; Nilvebrandt, L.; Hacksell, U. Antimuscarinic 3-(2-Furanyl)quinuclidin-2-ene Derivatives: Synthesis and Structure−Activity Relationships. *J. Med. Chem.* **1997**, *40*, 3804−3819.
(60) Corey, E. J.; Myers, A. G. Total Synthesis of (±)-Antheridium-Inducing Factor (AAn) of the Fern Anemia Phyllitidis. Clarification of Stereochemistry. *J. Am. Chem. Soc.* **1985**, *107*, 5574−5576.
(61) Chambers, R. D.; Hutchinson, J.; Sparrowhawk, M. E.; Sanford, G.; Moilliet, J. S.; Thomson, J. Elemental Fluorine Part 12. Fluorination of 1,4-Disubstituted Aromatic Compounds. *J. Fluorine Chem.* **2000**, *102*, 169−174.
(62) Li, J.; Norton, M. B.; Reinhard, E. J.; Anderson, G. D.; Gregory, S. A.; Isakson, P. C.; Koboldt, C. M.; Masferrer, J. L.; Perkins, W. E.; Seibert, K.; Zhang, Y.; Zweifel, B. S.; Reitz, D. B. Novel Terphenyls as Selective Cyclooxygenase-2 Inhibitors and Orally Active Antiinflammatory Agents. *J. Med. Chem.* **1996**, *39*, 1846−1856.
(63) Jendralla, H.; Chen, L.-J. Arylation of Phenols. Convenient, Regiospecific Methods for Mono- or Bis-*p*-Fluorophenylations, Suitable for Large Scale Syntheses. *Synthesis* **1990**, 827−833.
(64) Kelm, J.; Strauss, K. F−Nmr-Spectroscopy for the Identification of Photo Products Generated from Aromatic Iodo Compounds. *Spectrochim. Acta, Part A* **1981**, *37*, 689−692.
(65) Bumagin, N. A.; Bykov, V. V. Ligandless Palladium Catalyzed Reactions of Arylboronic Acids and Sodium Tetraphenylborate with Aryl Halides in Aqueous Media. *Tetrahedron* **1997**, *53*, 14437−14450.
(66) Ananthakrishnanadar, P.; Kannan, N. Kinetics of Reaction of Picryl Bromide with Substituted Biphenyl-4-Carboxylate Ions. *J. Chem. Soc., Perkin Trans. 2* **1982**, 1305−1308.
(67) Homsi, F.; Nozaki, K.; Hiyama, T. Solid-phase Cross-Coupling Reaction of Aryl(fluoro)silanes with 4-Iodobenzoic Acid. *Tetrahedron Lett.* **2000**, *41*, 5869−5872.
(68) Hajduk, P. J.; Dinges, J.; Miknis, G. F.; Merlock, M.; Middleton, T.; Kempf, D. J.; Egan, D. A.; Walter, K. A.; Robins, T. S.; Shuker, S. B.; Holzman, T. F.; Fesik, S. W. NMR−Based Discovery of Lead Inhibitors that Block DNA Binding of the Human Papillomavirus E2 Protein. *J. Med. Chem.* **1997**, *40*, 3144−3150.
(69) Patrick, T. B.; Willaredt, R. P. DeGonia, D. J. Synthesis of Biaryls from Aryltriazenes. *J. Org. Chem.* **1985**, *50*, 2232−2235.
(70) Kuchar, M.; Maturova, E.; Brunova, B.; Grimova, J.; Tomkova, H.; Holubek, J. Quantitative Relations Between Structure and Antiinflammatory Activity of Aryloxoalkanoic Acids. *Coll. Czech. Chem. Commun.* **1988**, *53*, 1862−1872.
(71) Allen, K. J.; Bolton, R.; Williams, G. H. Homolytic Reactions of Polyfluoroaromatic Compounds **16**. Competitive Phenylation of Polyfluorobenzenes. *J. Chem. Soc., Perkin Trans. 2* **1983**, 691−695.
(72) Nakada, M.; Miura, C.; Nishiyama, H.; Higashi, F.; Mori, T.; Hirota, M.; Ishii, T. Photoreactions of Polyhalobenzenes in Benzene−Formation of Terphenyls. *Bull. Chem. Soc. Jpn.* **1989**, *62*, 3122−3126.
(73) Weingarten, H. Steric Effects in the Gomberg Reaction. *J. Org. Chem.* **1961**, *26*, 730−733.
(74) Hashizume, H.; Ito, H.; Yamada, K.; Nagashima, H.; Kanao, M.; Tomoda, H.; Sunazuka, T.; Kumagai, H.; Omura, S. Synthesis and Biological-Activity of New 3-Hydroxy-3- Methylglutaryl Coenzyme-a (Hmg-Coa) Synthase Inhibitors−2- Oxetanones with a Side-Chain Mimicking the Folded Structure of 1233a. *Chem. Pharm. Bull.* **1994**, *42*, 512−520.
(75) Indolese, A. F. Suzuki-Type Coupling of Chloroarenes with Arylboronic Acids Catalyzed by Nickel Complexes. *Tetrahedron Lett.* **1997**, *38*, 3513−3516.

(76) Pridgen, L. N.; Snyder, L.; Prol, J. Transition-Metal Catalyzed Grignard Cross-Coupling to Ortho-Halogenated Aryl Imines—an Efficient Synthesis of Ortho-Substituted Aryl Aldehydes. *J. Org. Chem.* **1989**, *54*, 1523−1526.
(77) Huang, C. G.; Beveridge, K. A.; Wan, P. Photocyclization of 2-(2′-Hydroxyphenyl) Benzyl Alcohol and Derivatives Via Ortho-Quinonemethide Type Intermediates. *J. Am. Chem. Soc.* **1991**, *113*, 7676−7684.
(78) Wendeborn, S.; Berteina, S.; Brill, W. K.-D.; Mesmaeker, A. D. Palladium-Mediated C−C and C−S Bond Formation on Solid Support. A Scope and Limitations Study. *Synlett.* **1998**, *6*, 671−675.
(79) Stevens, C. V.; Peristeropoulou, M.; De Kimpe, N. Synthesis of 2,5-Difunctionalised-3,3-Dimethylpiperidines Via Omega-Halogenated Imines. *Tetrahedron* **2001**, *57*, 7865−7870.
(80) Tanaka, K.; Kishigami, S.; Toda, F. A New Method for Coupling Aromatic Aldehydes and Ketones to Produce α-Glycols Using Zinc−Zinc Dichloride in Aqueous Solution and in the Solid State. *J. Org. Chem.* **1990**, *55*, 2981−2983.
(81) Clive, D. L. J.; Kang, S. Z. Synthesis of Biaryls by Intramolecular Radical Transfer in Phosphinates. *J. Org. Chem.* **2001**, *66*, 6083−6091.

JM030347N